Chemistry - A European Journal

The important role of the nuclearity, rigidity and solubility of phosphane ligands on the biological activity of gold(I) complexes.

--Manuscript Draft--

Manuscript Number:	chem.201802547R1
Article Type:	Full Paper
Corresponding Author:	Laura Rodríguez Universitat de Barcelona Barcelona, SPAIN
Corresponding Author E-Mail:	laura.rodriguez@qi.ub.es
Order of Authors (with Contributor Roles):	Noora Svahn
	Artur J Moro
	Catarina Rodrigues
	Rakesh Puttreddy
	Kari Rissanen
	Pedro Viana Baptista
	Alexandra Fernandes
	João Carlos Lima
	Laura Rodríguez
Keywords:	gold(I); X-ray; antitumoral agents; ovarian carcinoma; intrinsic apoptosis
Manuscript Classifications:	Antitumor agents; Bioinorganic chemistry; Metal-metal interactions; Organometallic chemistry; Pi interactions
Abstract:	A series of 4-ethynylaniline gold(I) complexes containing monophosphanes (1,3,5-triaza-7-phosphaadamantane, PTA, 2; 3,7-diacetyl-1,3,7-triaza-5-fosfabiciclo[3.3.1]nonane, 3; and PR3, being R = naphtyl, 4; phenyl, 5 and ethyl, 6) and diphosphanes (bis(diphenylphosphino)acetylene, dppa, 7; trans-diphenylphosphineethene, dppet, 8; 1,2-bis(diphenylphosphino)ethane, dppe, 9; 1,3-bis(diphenylphosphino)propane, dppp, 10) ligands was synthetized and their efficiency against tumor cells evaluated. The cytotoxicity of complexes 2-10 was evaluated in human colorectal (HCT116) and ovarian (A2780) carcinoma, to the effect on normal human fibroblasts. All the complexes showed a higher antiproliferative effect in A2780 cells, with the following order of cytotoxicity: 5 > 6 = 9 = 10 > 8 > 2 > 4 > 7 > 3. Complex 4 stands out for a very high selectivity towards ovarian carcinoma cells (IC50 2.3 uM), compared to colorectal carcinoma and normal human fibroblasts (IC50 > 100 uM), making this complex very attractive for ovarian cancer therapy. Its cytotoxicity in these cells correlates with the induction of the apoptotic process and an increase of intracellular reactive oxygen species (ROS). The effect of the nuclearity, rigidity and solubility of the complexes on their biological activity was also analyzed. X-Ray crystal structures determination allowed the identification of short N-H···pi contacts as the main driving forces for the 3D packing in these molecules.
Response to Reviewers:	Barcelona, 15th July 2018 Dear Editor, Please, find enclosed the revised version of the manuscript entitled “The important role of the nuclearity, rigidity and solubility of phosphane ligands on the biological activity of gold(I) complexes”. We have considered the corrections and suggestions received from the referees and the manuscript has been modified and improved accordingly. All changes have been marked in red in this revised version. Answers to reviewers:

The important role of the nuclearity, rigidity and solubility of phosphane ligands on the biological activity of gold(I) complexes.

Noora Svahn,[a] Artur J. Moro,[b] Catarina Roma-Rodrigues,[c] Rakesh Puttreddy,[d] Kari Rissanen,[d] Pedro V. Baptista,[c] Alexandra R. Fernandes,[c*] João Carlos Lima,[b] Laura Rodríguez[a,e*]

[a] *Departament de Química Inorgànica i Orgànica. Secció de Química Inorgànica. Universitat de Barcelona, Martí i Franquès 1-11, 08028 Barcelona, Spain.*

[b] *LAQV-REQUIMTE, Departamento de Química, CQFB, Universidade Nova de Lisboa, Monte de Caparica, Portugal*

[c] *UCIBIO, Departamento de Ciências da Vida, Faculdade de Ciências e Tecnologia, Universidade Nova de Lisboa, Campus de Caparica, 2829-516 Caparica, Portugal*

[d] *University of Jyvaskyla, Department of Chemistry, Nanoscience Center, P.O. Box 35, 40014 Jyväskylä, Finland.*

[e] *Institut de Nanociència i Nanotecnologia (IN^{2}UB). Universitat de Barcelona, 08028 Barcelona (Spain)*

***corresponding authors**

Laura Rodríguez (laura.rodriguez@qi.ub.es)

Alexandra R Fernandes (ma.fernandes@fct.unl.pt)

Abstract

A series of 4-ethynylaniline gold(I) complexes containing monophosphanes (1,3,5-triaza-7-phosphaadamantane, PTA, **2**; 3,7-diacetyl-1,3,7-triaza-5-fosfabiciclo[3.3.1]nonane, **3**; and PR_3, being R = naphtyl, **4**; phenyl, **5** and ethyl, **6**) and diphosphanes (bis(diphenylphosphino)acetylene, dppa, **7**; trans-diphenylphosphineethene, dppet, **8**; 1,2-bis(diphenylphosphino)ethane, dppe, **9**; 1,3-bis(diphenylphosphino)propane, dppp, **10**) ligands was synthetized and their efficiency against tumor cells evaluated.

The cytotoxicity of complexes **2-10** was evaluated in human colorectal (HCT116) and ovarian (A2780) carcinoma, to the effect on normal human fibroblasts. All the complexes showed a higher antiproliferative effect in A2780 cells, with the following order of cytotoxicity: **5** > **6** = **9** = **10** > **8** > **2** > **4** > **7** > **3**.

Complex **4** stands out for a very high selectivity towards ovarian carcinoma cells (IC_{50} 2.3 μM), compared to colorectal carcinoma and normal human fibroblasts (IC_{50} > 100 μM), making this complex very attractive for ovarian cancer therapy. Its cytotoxicity in these cells correlates with the induction of the apoptotic process and an increase of intracellular reactive oxygen species (ROS).

The effect of the nuclearity, rigidity and solubility of the complexes on their biological activity was also analyzed. X-Ray crystal structures determination allowed the identification of short N-H···π contacts as the main driving forces for the 3D packing in these molecules.

Keywords: gold(I); X-Ray; antitumoral agents; ovarian carcinoma, intrinsic apoptosis

Introduction

Cisplatin and other platinum-based metal complexes such as carboplatin and oxaliplatin are the most widely used and efficient anticancer drugs for the treatment of testicular, ovarian and bladder cancer. However, the clinical success of cisplatin and its derivatives is compromised due to inevitable serious side effects, such as nephrotoxicity and neurotoxicity, ototoxicity and development of drug resistance.[1] Therefore, interest in medicinal inorganic chemistry has continued to grow with the emergence of gold complexes as alternatives to cisplatin, as many gold(I) and gold(III) compounds exhibited potent tumor cell growth inhibitory properties with much lower toxicity and fewer side effects.[2-5] The recent interest in the biochemistry and bio-inorganic chemistry of gold has triggered a flood of reports on the use of gold complexes as potential treatment for a variety of disease models, including rheumatoid arthritis and other chronic inflammatory and auto-immune diseases, various cancers, as well as bacterial, fungal and viral infections.[6] Most of these reports focus on gold in either +I or +III oxidation states, as these forms are comparatively stable in aqueous solution, facilitating their use in biological research.[7-12] Among the gold complexes with potential anticancer effect, Auranofin (Ridaura®), a glucopyranosato triethylphosphine gold(I) complex, commonly used in clinical practice to treat rheumatoid arthritis, has showed a promising effect in the treatment of several types of cancer (e.g. including ovarian cancer ClinicalTrials.gov Identifiers: NCT01747798 and NCT03456700). The potential impact of auranofin triggered the development of new gold compounds. It is known that auranofin and gold(I) phosphine related compounds selectively inhibit the mitochondrial thioredoxin reductase, leading to increased ROS production, and consequent mitochondrial damage followed by internal induction of apoptosis.[13-16] Since the mechanisms of action of anticancer gold complexes are likely to be different from those of cisplatin, most of the reported cytotoxic gold complexes are also effective against cisplatin-resistant cancer cells, revealing the promising prospect in the development of gold chemotherapeutics to resolve the problem of cisplatin resistance.[17] Ligand displacement is an important reaction of gold(I) complexes in biological systems. Additionally, this auxiliary ligand can affect the compounds lipophilicity, stability and the binding affinity of gold(I), and hence the intracellular transformation of gold(I) species under both *in vitro* and *in vivo* conditions. For this reason, lipophilic/hydrophilic balance should be adjusted through ligand design.

Gold(I) forms linear complexes, where phosphines[18] and N-heterocyclic carbenes[19] represent the most common ligands. Thus, complexes containing Au-P bond play an important role in coordination and organometallic chemistry in the last years. The great interest for this class of complexes is accounted not only for "pure chemistry" aspects but also for their applications in homogeneous catalysis,[20] development of anticancer and antimicrobial metallodrugs and luminophores.[2,3,21] While monodentate tertiary phosphine ligands have found broad application in the development of anti-cancer gold complexes, the use of diphosphine ligands is not so extensively exploited.[3,22]

On the other hand, there has been increasing interest over the last 20 years in gold(I) organometallic complexes containing alkynyl units because of their potential application in different fields in chemistry, such as molecular electronics, chemical sensors, materials science, supramolecular chemistry and biological activity among others.[23-27] Nevertheless, their anticancer activity is just increasing on interest in the last years and the results are quite promising.[3,28-38]

Taking into consideration all these facts, we have analyzed the effect of the phosphane unit in the corresponding biological activity of a series of gold(I) complexes containing the same 4-ethynylaniline chromophore at the second coordination position. Different factors have been herein considered: i) changes on the solubility of the phosphine in water; ii) changes on the aromaticity of the PR_3 substituents (being R = Ph, Naph or ethyl); iii) the nuclearity of the complexes (by using diphosphines instead of monophosphines); iv) flexibility of the molecules (rigid vs. flexible diphosphines). The observed biological activity in different cancer cell lines has been correlated with the differences on the resulting chemical structure to obtain some structure-activity-relationship information. The mechanism underlying cytotoxicity/selectivity for ovarian carcinoma cells of the most promising complex was further characterized.

Results and Discussion

Synthesis and Characterization

The reaction of a dichloromethane suspension of $[Au(C{\equiv}CC_6H_4NH_2)]_n$ (**1**) with either 1 equivalent of PTA, DAPTA, $PNaph_3$, PPh_3, PEt_3 or 0.5 equiv of dppa, dppet, dppe and dppp afforded the desired complexes $[Au(C{\equiv}CC_6H_4N)(PR_3)]$ (**2**-**6**) and $[Au_2(C{\equiv}CC_6H_4NH_2)_2(\mu^2\text{-diphosphine})]$ (**7**-**10**) in a yield greater than 60% yield (Schemes 1 and S1-2).

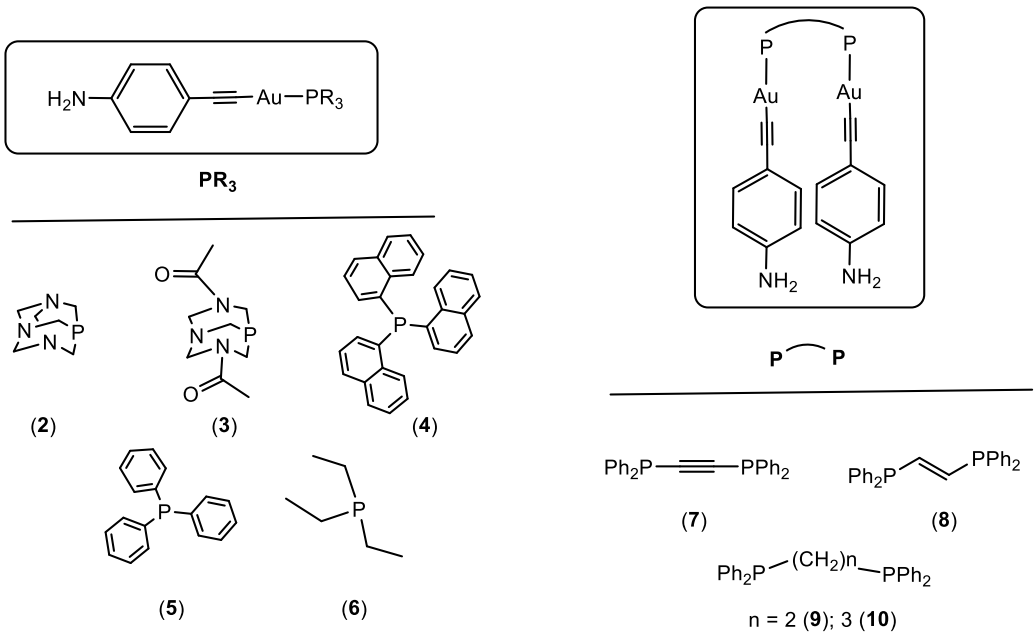

Scheme 1. Chemical structure of the mononuclear (**2**-**6**) and dinuclear complexes (**7**-**10**) synthesized in this work.

All the synthesized complexes gave satisfactory elemental analysis and were characterized by ^1H and ^{31}P spectroscopy, ESI-MS(+) spectrometry and IR spectroscopy. $^{31}P\{^1H\}$ NMR display in all cases a single resonance, which is *ca*. 50 downfield in comparison with the free phosphine.[28,34,36-41] Only one peak was recorded for the diphosphine derivatives **7**-**10** in agreement with the formation of the symmetrical dinuclear complexes (see Supporting Information).

^1H NMR spectra show the expected signals for α and β protons of the aniline rings as well as the protons attributable to the phosphine ligands. The characteristic vibration of the $\bar{\upsilon}(C{\equiv}C)$ at *ca*. 2100 cm^{-1} is also observed by IR spectroscopy. This band is slightly shifted

to higher energies with respect to the polymer **1**, as previously observed for other derivatives with analogous chemical structure.[34,40,41] The presence of the molecular peak recorded in all cases by ESI-MS spectrometry confirms definitively the successful formation of all complexes.

In order to try to find out the effect of the phosphine conformation of **8** on the chemical structure and the resulting biological properties, attempts to synthesize the corresponding *cis*-phosphine gold(I) isomer were performed. In sharp contrast with the other phosphines, when the gold polymer $[Au(C{\equiv}CC_6H_4NH_2)]_n$ (**1**) was reacted with *cis*-dppet (*cis*-1,2-bis(diphenylphosphino)ethene) in a molar ratio 1:1, under the same conditions as reported above, a mixture of three different products were obtained being identified as the ionic compound $[Au(cis\text{-}dppet)_2][Au(C{\equiv}CC_5H_4NH_2)_2]$ (Scheme S3) in coexistence with the desired product and complex **8**. This is supported by ^{31}P NMR characterization (Figure S19) and the ESI-MS analysis that displays the peaks at m/z 989.2 ($[Au(cis\text{-}dppet)_2]^+$) and 626.02 ($[Au(C{\equiv}CC_5H_4NH_2)_2]^-$) in negative and positive mode. Changes on the concentration and/or the reaction time did not have any influence on the resulting chemical composition.

In order to obtain complexes with higher solubility in water, similar reactions were performed by using 3-(diphenylphosphanyl)propanoic acid (Scheme S4-**a**) and 4-(diphenylphosphanyl)benzoic acid (Scheme S4-**b**) but the resulting products could not be obtained in pure form in agreement with NMR data. A mixture of products can be identified according to the presence of several peaks in the ^{31}P NMR (Figures S20-S21) that could not be consequently isolated and purified. This could be attributed to the possible coordination of the oxygen to the gold metal atom[42-44] giving rise to different type of derivatives (P-coordination and O-coordination) with similar polarity that precludes their purification. Final attempts were performed by the synthesis of the corresponding phosphine potassium salts. The reaction of 4-(diphenylphosphanyl)benzoic acid with KOH gave $KPPh_2C_6H_4CO_2$ (**11**), which was characterized by ^1H and ^{31}P NMR, IR and ESI-MS. Approximately 1.5 ppm downfield shifted signal in ^{31}P NMR, the absence of O-H and C=O vibration in the IR spectrum and the appearance of characteristic band at 1587 and 1394 cm^{-1} [45] are in accordance with the presence of COO^- ion. The reaction of 3-(diphenylphosphanyl)propanoic acid with KOH did not give pure $KPC_{15}H_{14}O_2$, which was proved by ^{31}P NMR showing two different signals. Unfortunately, the reaction of **11** with AuCl(tht) in dichloromethane

gave a mixture of products including decomposition of gold(I) complex. Therefore, no pure anionic chloro-gold(I) complex could be isolated from these reactions and thus, the resulting aniline products were not possible to obtain.

The solid-state structures of **4**, **8**, **9** and **10** were analyzed through single crystal X-ray diffraction studies (Figure 1). Slow evaporation of the dichloromethane/hexane solution provides single crystals suitable for X-ray crystallography. The complex **8** formed very low quality and badly twinned single crystals and resulted in abnormal bond distances in the second Au-PPh_3 moiety, thus only the overall structure (dimer) and the Au···Au distances in **8** can be considered reliable (See Supporting Information Fig. S24 for X-ray crystal structure of **8**). Attempts to obtain crystals for other complexes were unsuccessful. The coordination of acetylene ligands at the Au(I) centers are linear, the P–Au–C angles range between 170.9(3)° and 179.1(1)°. The Au(I) centers in **4**, **9** and **10** adopt linear geometries and **8** has a T-shape geometry. The P–Au and Au–C bond parameters are in good agreement with previously reported Au(I)-acetylide complexes.[23,46,47] All four complexes display, tetrahedral geometry at hinge phosphorus atom, near linear geometry of P–Au–C≡C–C units and, typical N–H···C_{sp}, C–H···π and π–π interactions in the 3-D crystal packing similarly to previously reported gold(I) complexes. [23,46,47] The analysis of short contacts in complexes **4**, **8**, **9** and **10** in particular N–H···C_{sp} were analysed using Hirshfeld surfaces. [48-50] The red spots in Fig. S25-S29 (see Supporting Information) indicate of short contacts between -NH_2 and Au(I) bound acetylenic groups.

Complexes **4** and **10** are discrete structures, while **8** and **9** form dimers by aurophilic interactions as shown in Figures 1 and S24. The packing arrangement in **4** and reported [Au(C≡C-$C_6H_4NH_2$){P(3-tolyl)$_3$}][29] are remarkably similar (Fig. S30), both form 1-D zig-zag polymeric structures, with N–H···C_{sp} interactions (*ca*. 2.39 and 2.67 Å) connect discrete units of **4**, while the [Au(C≡C-$C_6H_4NH_2$){P(3-tolyl)$_3$}] units extend *via* N–H···Au interactions. The *trans*- and *anti*- orientation of backbone P–C–C–P in **9** is the major structural feature responsible for dimerization *via* Au···Au interactions. In **8**, the dimers stabilize through cooperative weak Au···Au interactions [3.316(2) Å] as shown in Figure S24. In complex **9**, acetylenic moieties are positioned in the direction similar to chloride ligands in [Au_2Cl_2(dppe)]. [51] The Au···Au interactions [3.118(1) Å] in **9** are similar to [Au_2Cl_2(dppe)] [3.162(2) Å][51] and shorter when compared to **8** [3.316(2) Å]. The shorter Au···Au interactions in **9** are perhaps due to flexible ligand, dppe, compared to rigid and planar dppet. The C–H_{Ar}···C_{sp} interactions link the dimeric structures in the

3-D crystal packing of **9** (Fig. S31). In dppp, the more flexible propane chain between two phosphorus atoms has ability to exhibit various conformers.[52-59] In complex **10**, the propane chain adopts *anti-anti* conformation with two P–Au–C≡C–C units roughly parallel to each other with Au(I) ions separated at distances, *ca*. 5.60 Å. The intermolecular N–H···C≡C interactions between $–NH_2$ and C≡C groups of discrete units **10** ranging between *ca*. 2.44 and 2.56 Å play significant role in stabilizing the 3-D lattice. (Fig. S32) Similar type N–H···C≡C interactions were previously reported between aniline and dppp-Au(I) macrocyclic compounds.[60] Of note, the 3-D crystal packing of **10** reveals a complex pattern of numerous short contacts, of prominent were N–H···C_{Ar}, dichloromethane incorporated C–Cl···π and C–H···π interactions (Fig. S27-S29).

Photophysical Characterization

Absorption and emission spectra of all the complexes were recorded in $2 \cdot 10^{-5}$ M solutions at room temperature and the obtained data are summarized in Table 1.

The electronic absorption spectra of all complexes (Figure 2) show intense high-energy bands at *ca*. 300 nm and low energy bands or tails at *ca*. 353-400 nm. The higher energy band display the same profile as the corresponding spectrum of the 4-ethynylaniline ligand (Figure S33), which is red shifted due to the coordination to the metal atom and it is thus assigned to $\pi - \pi^*$ transition of the ethynylaniline moiety. Additionally, as observed for ethynylaniline, is *ca*. 20 nm red-shifted in the case of THF/H_2O mixtures (compounds **4**-**10**) with respect to pure water solutions (compounds **2** and **3**).

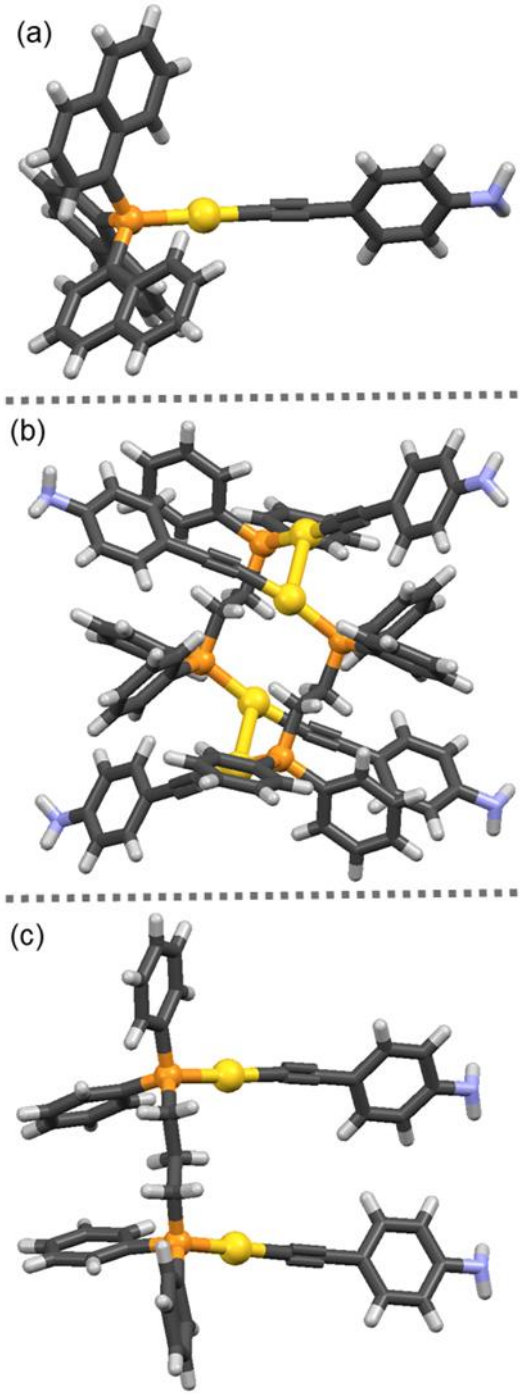

Figure 1. X-Ray crystal structure of **4** (a), **9** (b) and **10** (c). Yellow: gold; orange: phosphorus; black: carbon; light blue: nitrogen; Solvents are omitted for viewing clarity. (See Supporting Information Fig. S24 for X-ray crystal structure, **8**).

Table 1. Absorption and emission spectral data of 4-ethynylaniline and complexes **2-10** in water (**2-3**) and 1: 1 THF:H_2O (**4-10**). [a] H_2O; [b] H_2O/THF 1:1; λ_{exc} = 285 nm for **2** and **3**); λ_{exc} = 310 nm (for **4-10**)

Compound	**Absorption λ_{max}(nm) ($10^{-3}\varepsilon$ (M^{-1} cm^{-1}))**	**Emission λ_{max}(nm)**
4-ethynylaniline	265 (28.3)[a], 277 (32.7)[b]	355
2	290 (16.0)	352, 470
3	292 (19.5)	354, 459
4	298 (41.1), 381 (6.7)	342
5	315 (18.4)	353
6	310 (20.9)	358
7	307 (20.7), 404 (14.4)	350, 420
8	314 (25.7), 400 (4.5)	350, 420
9	313 (19.9), 382 (11.9)	350, 420
10	310 (22.0), 380 (2.7)	350, 420

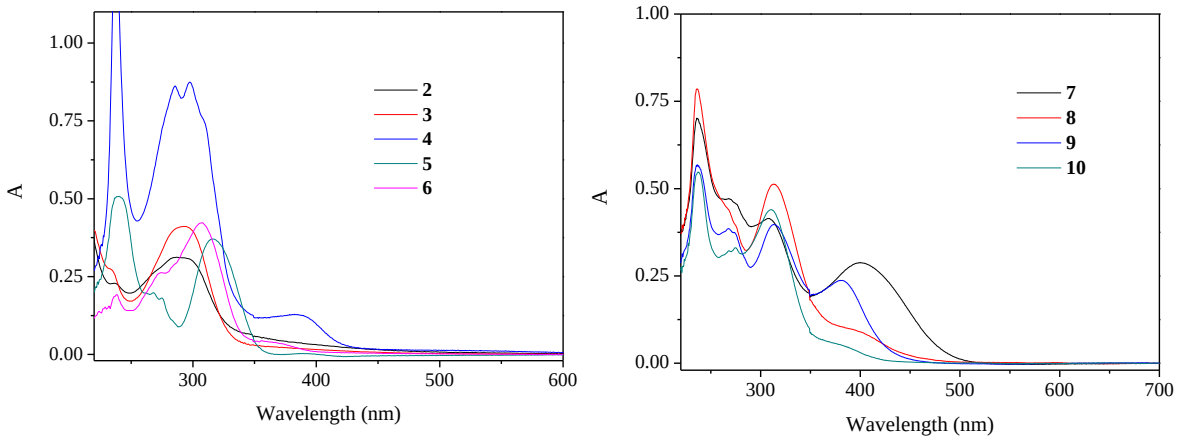

Figure 2. Absorption spectra of $2 \cdot 10^{-5}$M solutions of mononuclear (left) and dinuclear (right) complexes in water (**2-3**) and 1: 1 THF:H_2O (**4-10**). Different colors represent each compound as indicated in the figure.

A particular shape is recorded in the case of **4** containing the tris-naphthylphosphine ($PNaph_3$) with an absorption band centered at 298 nm overlapping the absorption of the ethynylaniline group and presents a higher intensity and vibronically structured band, typical of C=C aromatic moieties and is ascribed to the π-π* ($Naph_3$) transition. The lower energy absorption band *ca*. 400 nm is observed as a tail in some cases has been assigned to aggregates' absorption from σ*(Au···Au)–π* transitions.[61]

Emission spectra recorded upon excitation at *ca*. 300 nm displays a highly energy emission at 350 nm tentatively assigned to $^1[\pi–\pi^*$(ethynylaniline)] transition.[62] A lower energy band at 415-450 nm with lower intensity assigned to $^3[\pi–\pi^*$(ethynylaniline)] emission is observed in some cases (Figures 3 and S34-35). This phosphorescence emission seems to be more favored in the case of PTA and DAPTA derivatives (complexes **2** and **3**) probably due to the presence of aggregates with a direct influence on the aniline intersystem crossing process.

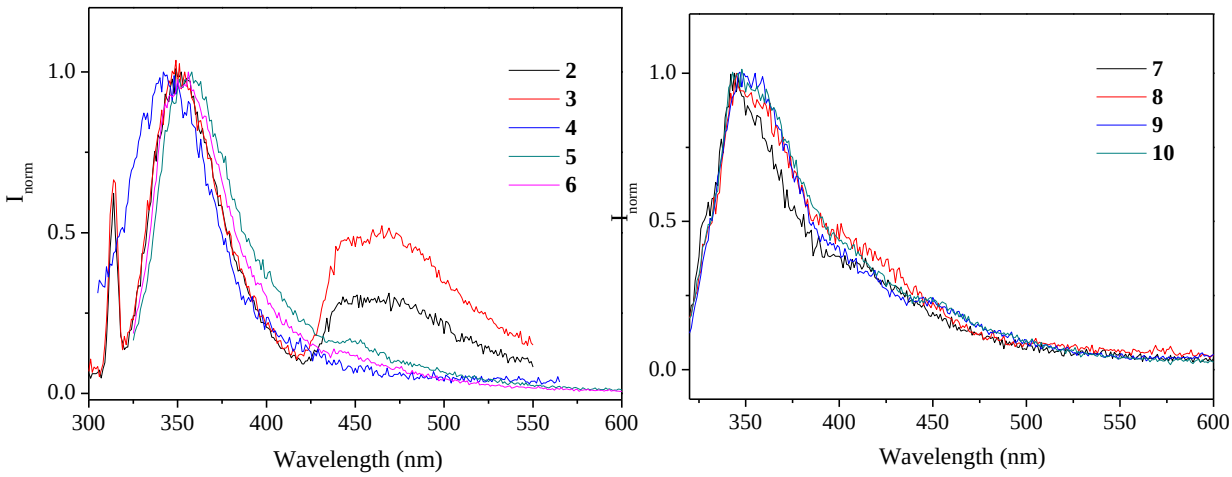

Figure 3. Normalized emission spectra of $2\cdot10^{-5}$M solutions of mononuclear (left) and dinuclear (right) complexes in water (**2**-**3**, λ_{exc} = 300 nm) and 1: 1 THF:H_2O (**4**-**10** λ_{exc} = 310 nm).

Biological assays

Cell viability

The cytotoxicity of the complexes and of each ligand were assessed by the MTS assay on representative human cancer cell lines: ovarian cisplatin sensitive, A2780; colorectal carcinoma, HCT116. Except for trans-dppet, dppe and dppp, the ligands of the dinuclear

complexes, trans-dppet, dppe and dppp no cytotoxic effect was observed for the other ligands in concentrations up to 100 μM (Figure S36, Table S2). A concentration dependent effect on cell viability was observed after 48 h incubation for all complexes in both cancer cell lines. An exception is complex **4**, where the IC_{50} in HCT116 cells was higher than 100 μM (Figure 4, Table 2).

Table 2. Relative IC_{50} (μM) for complexes **2-10** in the human cancer cell lines (A2780, HCT116) and in normal human fibroblasts (48 h).

IC_{50} (μM)	**A2780**	**HCT116**	**Fibroblasts**
Complexes			
2	1.7 ± 0.4	18.2 ± 8.1	19.0 ± 7.3
3	17.4 ± 1.0	77.5 ± 0.1	70.4 ± 3.5
4	2.3 ± 0.1	> 100	> 100
5	0.1 ± 0.0	8.7 ± 1.8	5.3 ± 0.7
6	0.3 ± 0.1	6.5 ± 0.1	1.0 ± 0.4
7	10.9 ± 3.7	59.5 ± 17.5	96.3 ± 4.5
8	0.4 ± 0.2	4.9 ± 0.2	36.4 ± 1.2
9	0.3 ± 0.0	1.9 ± 0.3	15.2 ± 1.8
10	0.3 ± 0.1	1.3 ± 0.0	36.4 ± 0.0

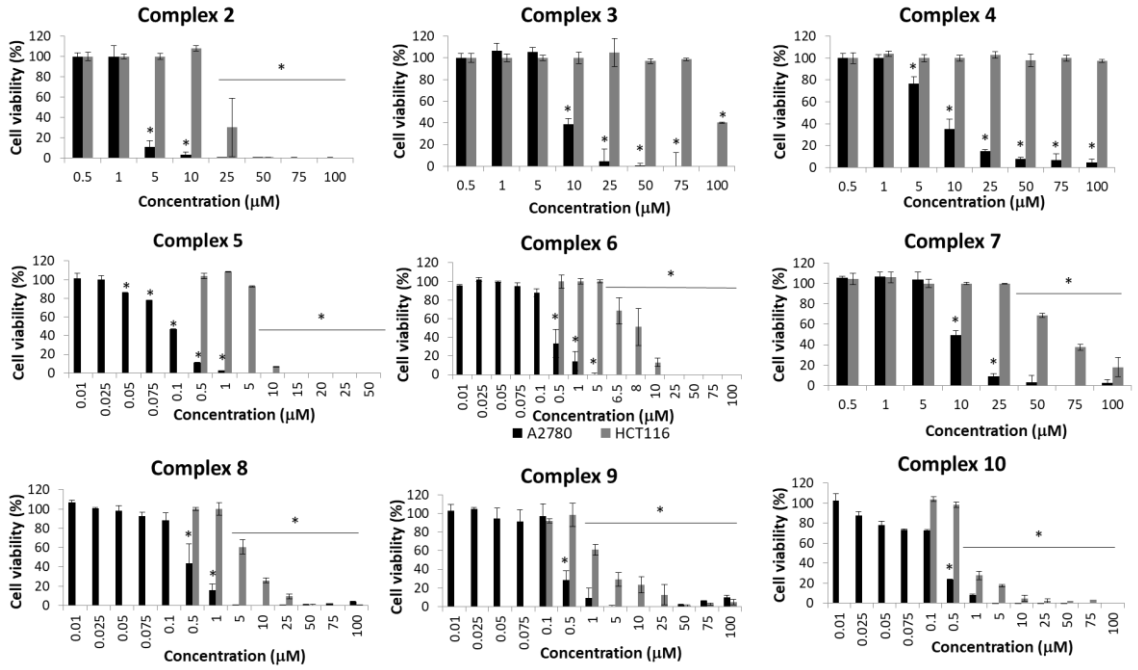

Figure 4. Cytotoxicity of complexes **2-10** in A2780 cell line (black bars) and HCT116 cell line (grey bars) after 48 h incubation with increasing concentrations of the complex. Cell viability was determined by MTS assay. Data normalized against the control (0.1 % (v/v) DMSO) and expressed as mean ± SEM of three independent assays. * $p < 0.05$ relative to control for each cell line.

The effect of the mononuclear complexes **2-6** shows a similar trend in cell viability, and the IC_{50} values for A2780 are at least 10 times lower than those for HCT116. This suggests a considerable selectivity of the mononuclear gold(I) complexes towards ovarian carcinoma cells. Complex **4**, containing tri-1-naphtylphosphine, stands out due to the higher difference observed between cytotoxicity in A2780 (IC_{50} 2.3 μM) relative to HCT116 (IC_{50} > 100 μM). The cytotoxic effect of mononuclear complexes on primary human fibroblasts is in the same order of magnitude of that on HCT116 cancer cell line (Figure 5, Table 2).

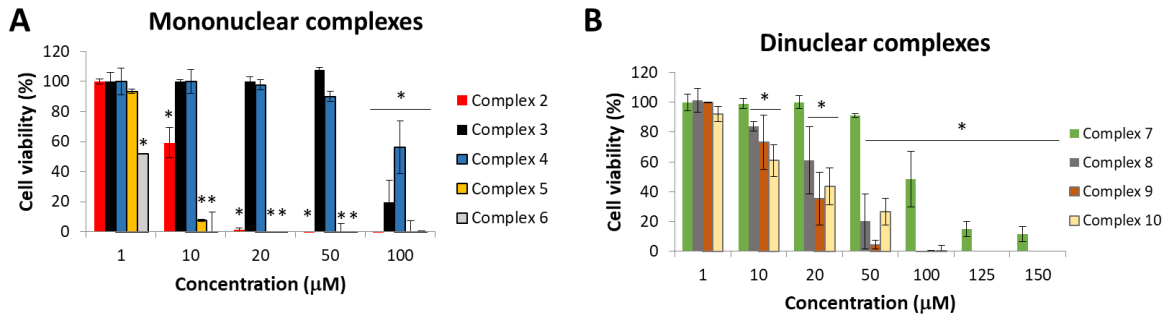

Figure 5. Cytotoxicity of complexes **2-10** in normal human fibroblasts determined by MTS assay. Fibroblasts were challenged with increasing concentrations of A) mononuclear complexes **2** (red bars), **3** (black bars), **4** (blue bars), **5** (yellow bars), and **6** (light grey bars), and B) dinuclear complexes **7** (green bars), **8** (dark grey bars), **9** (brown bars) and **10** (light brown bars) after 48 h incubation. Data normalized against the control (0.1 % (v/v) DMSO) and expressed as mean ± SEM of three independent assays. * $p < 0.05$ relative to control for each cell line.

Complex **2** (containing PTA) showed a lower IC_{50} than complex **3** (containing DAPTA), suggesting that gold(I) coordination with PTA ligand leads to higher cytotoxicity than DAPTA in A2780 cells (Table 2) as previously observed in other gold(I) alkynyl complexes that differ on these phosphanes.[34] However, complex **3** showed lower cytotoxicity towards healthy human fibroblasts (IC_{50} 70.4 μM) compared to complex **2** (IC_{50} 19.0 μM) (Figure 5, Table 2). Interestingly, previous analysis of gold(I) complexes containing DAPTA and PTA in combination with thionate ligands revealed cell growth inhibition of the cisplatin sensitive cell line A2780 with similar IC_{50} at 72 h.[28,63]

Our data indicate that, among the mononuclear compounds, complex **5**, with PPh_3, and complex **6**, which like auranofin is combined with PEt_3, showed the highest antiproliferative activity in A2780 cell line. Moreover, cytotoxicity in A2780 cells of complex **6** (IC_{50} 0.3 ± 0.1 μM after 48h) is slightly higher than that of auranofin (0.5 ± 0.1 μM after 72h).[64] Despite this higher cytotoxicity in A2780 tumor cell line, the IC_{50} of both compounds in healthy fibroblasts at 48 h is lower than the corresponding value for complex **4**. These data seem to indicate that the latter is a more attractive complex for ovarian cancer therapy, as it allows the use of a higher concentration range with lower toxicity to normal cells (no effect on cell viability for concentrations up to 100 μM).

Concerning dinuclear complexes **7-10**, a decrease of cell viability was observed for the two tumor cell lines and healthy human fibroblasts in a concentration-dependent manner. Cytotoxicity of complexes **8-10** follow the same trend, with IC_{50} ranging from 0.3 to 0.4 μM in A2780 cells, 1.3 to 4.9 μM in HCT116 cells and 15.2 to 36.4 μM in human healthy fibroblasts. With the exception of complex **7**, the dinuclear complexes showed a higher cytotoxic effect in HCT116 cells compared to the mononuclear complexes **2-6**, independently of the ligand. This higher cytotoxicity of dinuclear complexes is correlated with the higher cytotoxicity of their respective ligands (Figures 4, 5, S36, Tables 2 and S2). Nevertheless, the dinuclear complexes **8-10** showed a higher cytotoxicity in normal healthy fibroblasts compared to their respective ligands, demonstrating their lower applicability due to the higher possible side-effects in healthy cells.

The flexibility of phosphine conformation showed to have a direct influence on the biological activity of the complexes. The higher rigidity of **7**, conferred by a triple bond between phosphines (Scheme 1), resulted in an increase of the IC_{50} for both cancer cell lines, when compared to the other dinuclear complexes **8-10** (Table 2).

Concerning the cellular uptake of the mononuclear complexes by A2780 cells, results suggested a correlation between IC_{50} and complex intracellular concentration, with higher Au concentrations for complex **5** treated cells (7.2 % Au, IC_{50} 0.1 μM) and lower Au for complex **3** treated cells (0.3 % Au, IC_{50} 17.4 μM) (Table 2, S3). This correlation can be translated to dinuclear complexes, where a lower toxicity correlates with intracellular concentration of the complex 7, probably due to the rigidity of the bond between the phosphines (Scheme 1, Table S3). However, when comparing mononuclear and dinuclear complexes, a much higher Au concentration in cells treated with complexes **8-9** was observed, reaching 46.7 % of intracellular gold in complex **8**, with IC_{50} 0.4 μM (Table 2, S3).

Considering the intracellular concentration of all the complexes, one might postulate that mononuclear compounds show higher cytotoxicity than the dinuclear counterparts because higher intracellular concentrations of dinuclear compounds resulted in similar IC_{50} compared to mononuclear complexes. For example, the mononuclear complex **6** and dinuclear complex **9** have identical IC_{50} (0.3 μM) but an intracellular gold concentration of 4.0 % and 41.7 %, respectively (Table 2, S3).

As such, complex **4** was selected for further biological characterization due to its higher specificity in A2780 tumor cell line and low toxicity in normal cells (high therapeutic index).

In a first approach, we took advantage of complex **4** fluorescence (excitation and emission wavelengths 310/410 nm, respectively in Tris-HCl 5 mM, pH 7.0, NaCl 50 mM) to evaluate the uptake by A2780 cells. A 2.5-fold increase of fluorescence intensity in cells treated with complex **4** compared to the non-treated cells was observed after a 3 h incubation, suggesting its fast internalization in A2780 cells (Figure 6). These observations corroborate and support the cell uptake data. Interestingly, after 6 h incubation, a decrease in fluorescence intensity of treated cells to the level of the control cells suggests that ligand displacement might have occurred within the cells or that the complex has been cleared (*e.g.* by efflux transporters). Both effects have been described for gold(I) complexes in colorectal and ovarian carcinoma cells.[65,66]

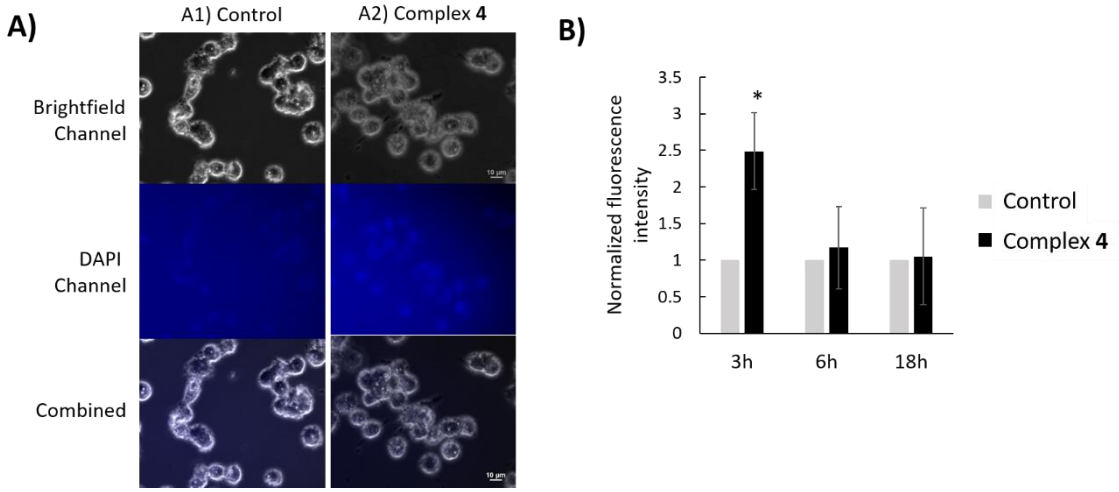

Figure 6. Internalization of complex **4** in A2780 cells. A) A2780 cells were incubated for 3 h with RPMI 1640 medium supplemented with 10 % (v/v) fetal bovine serum and A1) 0.05 % (v/v) DMSO (control) and A2) 10 x IC_{50} at 48 h of complex **4**. After replacing the medium with phosphate buffer saline cells were immediately visualized on a Ti-U Eclipse inverted microscope (Nikon, Tokyo, Japan) with DAPI filter cube (Nikon) (excitation filter of 340-380 nm and barrier filter at 435-485 nm). B) Fluorescence intensity of A2780 cells incubated for 3 h, 6 h and 18 h with control (grey bars) and 10 x IC_{50} at 48 h of complex **4** (black bars). Fluorescence intensity of cells was corrected with background fluorescence and normalized to the equivalent of cells

challenged with vehicle only (DMSO). Error bars represent SEM of 5 independent images with at least 10 cells per image. * p-value < 0.05 relative to the value of NS-023 treated cells for 6h and 18h.

Hoechst 33258 shows a high affinity to DNA, allowing to detect nuclear modifications induced by apoptosis, including chromatin condensation or nuclear fragmentation that ultimately lead to cell death.[67] So, a preliminary analysis was performed using this strategy to understand whether the decrease in A2780 cells viability by complex **4** was in fact due to apoptosis, i.e. cell death. Results show that after 9 h incubation with complex **4**, an increased number of nuclei showed apoptotic events (Figure 7), that agrees with the internalization results of complex **4** in A2780 cells and its induced cytotoxicity (Figures 4 and 6).

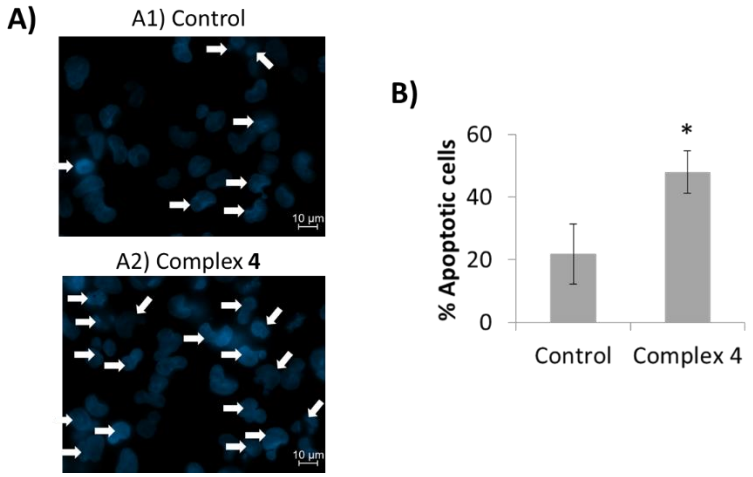

Figure 7. Apoptotic morphological changes in A2780 cells treated with complex **4**. A) Representative images of A2780 cells incubated for 9 h with RPMI 1640 medium supplemented with 10 % (v/v) fetal bovine serum and A1) 0.05 % (v/v) DMSO (control) and A2) the IC_{50} value at 48 h of complex **4** and stained with Hoechst 33258 for visualization of apoptotic nuclei (excitation and fluorescence emission at 352 nm and 461 nm, respectively). Three random microscopic fields with circa 30 nuclei were photographed using an AXIO Scope (Carl Zeiss, Oberkochen Germany). White arrows point to typical morphological features of apoptosis, including chromatin condensation and nuclear fragmentation. B) Percentage of apoptotic cells after 9 h incubation of A2780 cells with complex **4** and respective vector control. * p-value < 0.05 relative to the control sample.

The cytotoxic mechanisms of auranofin in tumor cells are not totally understood, but it is generally accepted that these involve the induction of intrinsic apoptosis triggered by increased oxidative stress due to inhibition of thioredoxin reductase.[13,14] As such, the induction of apoptosis by complex **4** was evaluated by calculating the apoptotic index, BAX/BCL-2 ratio. Intrinsic apoptosis is regulated by the BCL-2 family of proteins that is composed by pro-apoptotic proteins, such as BAX, and by anti-apoptotic proteins, such as BCL-2.[68] An increased BAX/BCL-2 ratio is indicative of increased intrinsic apoptosis.[68] After 3 h incubation, no alterations were registered. However, at 18h, the apoptotic index increased almost 2 times in complex **4** treated cells relative to the control (Figure 8). An increased apoptosis index was also observed at 48 h (Figure 8C). Together, these data indicate that cell death is triggered by apoptotic events in line with those observed of auranofin.

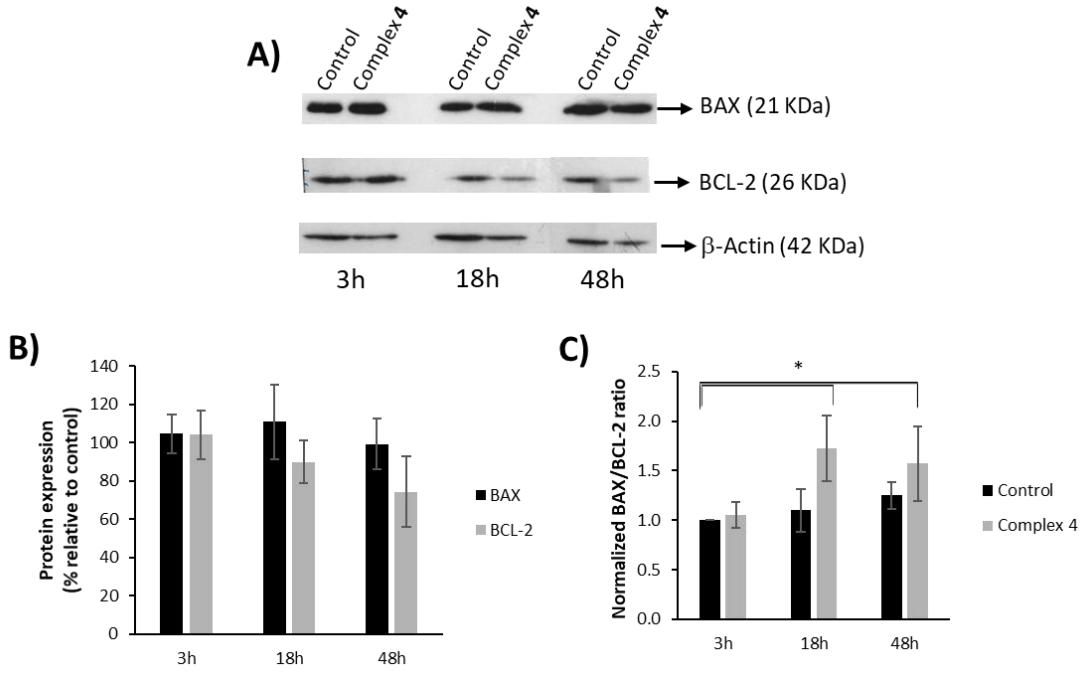

Figure 8. Expression of BAX and BCL-2 proteins after A2780 cell line incubation with complex **4**. A) Western-Blot for quantification of BAX, BCL-2 and β-actin in A2780 cell line after incubation for 3 h, 18 h and 48 h with IC_{50} at 48 h of 0.05 % (v/v) DMSO (control) or complex **4**. Protein band intensity was first normalized against β-Actin and then with sample incubated for 3 h with DMSO. B) Protein expression of BAX (black bars) and BCL-2 (grey bars). C) Apoptotic index of A2780 cells, calculated by BAX/BCL-2 ratio, after incubation with control (black bars) and complex **4** (grey bars). * p-value < 0.05 (obtained by t-test analysis).

To further corroborate this intrinsic apoptotic event, the mitochondrial membrane potential was evaluated. Mitochondrial membrane permeabilization, which mainly consist in dissipation of mitochondrial potential and increased production of ROS, is initiated by pro-apoptotic members of the BCL-2 protein family and is the point of no return in the events that lead to intrinsic apoptosis.[69] The mitochondrial membrane potential was assessed by calculating JC-1 monomer/aggregate ratio. JC-1 is a green fluorescence dye that, when accumulates at the mitochondrial matrix with an intact electrochemical gradient, suffers a red-shift of the emission peak.[70]

Dissipation of the mitochondrial membrane potential, was observed after 48 h incubation of A2780 cells at IC_{50} of complex **4** (Figure 9). Interestingly, mitochondria hyperpolarization was observed after 3 h and 18 h incubation, regardless of some heterogeneity.

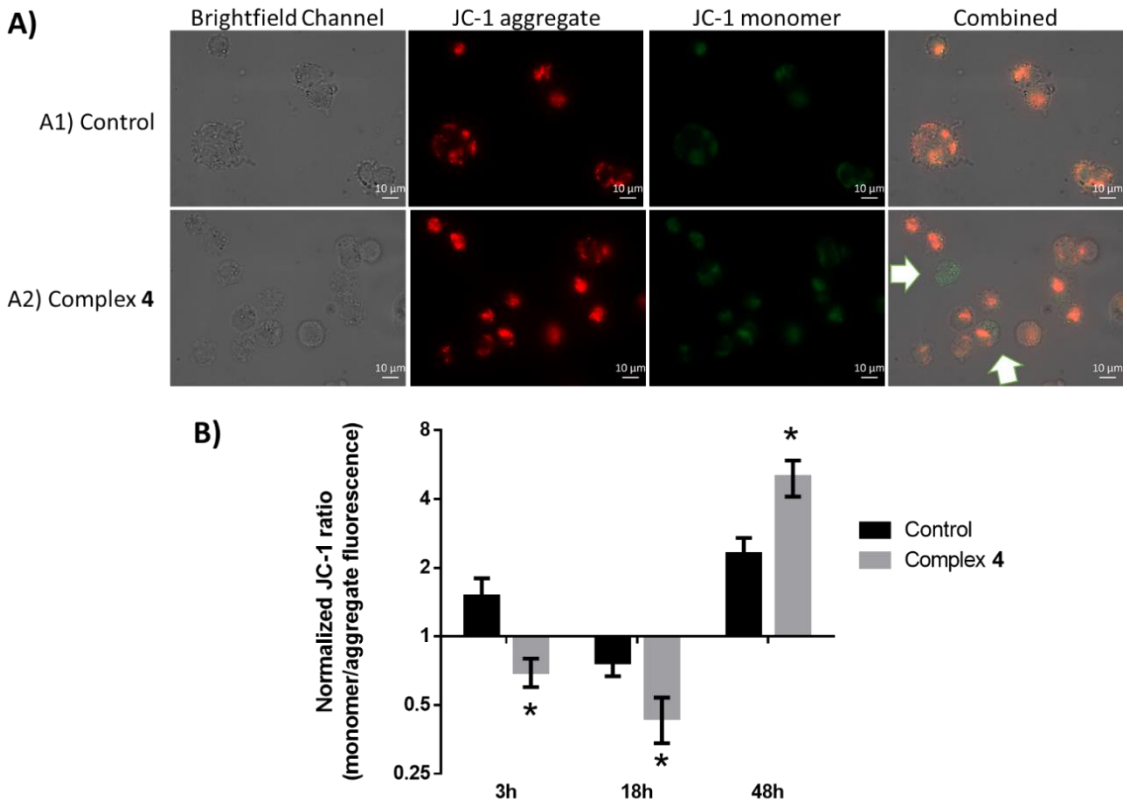

Figure 9. Mitochondrial membrane potential of A2780 treated with Complex **4** evaluated by the measurement of JC-1 fluorescence. A) A2780 cells were incubated for 3 h with RPMI 1640 supplemented with 10 % (v/v) fetal bovine serum and A1) 0.05 % (v/v) DMSO (Control) and A2) IC_{50} at 48 h complex **4** and stained with JC-1. Five random microscopic fields with circa 30 nuclei were photographed using an AXIO

Scope (Carl Zeiss, Oberkochen Germany) using for the same field brightfield image acquisition, rhodamine fluorophore settings (excitation and emission wavelength 540 / 570 nm, respectively) for JC-1 aggregate conformation (JC-1 aggregate), and FITC settings (excitation and emission wavelength 485 / 535 nm, respectively) for image acquisition of the monomer conformation (JC-1 monomer). White arrows point to cells with different membrane potential than the overall cells in the image. B) JC.1 ratio of monomer vs aggregate fluorescence obtained after 3 h, 18 h and 48 h incubation of A2780 cells. Values were normalized to the JC-1 ratio of untreated cells. * p-value < 0.05 relative to the value of DMSO at the same time point.

In line with results obtained for mitochondrial potential, ROS production in A2780 cells under the same experimental conditions increased significantly after 48 h incubation (Figure 10). These findings suggest that, unlike auranofin, where an increase of ROS at the first hours of incubation is observed due to an impairment of thioredoxin reductase activity which in turn triggers apoptosis, in the presence of complex **4,** the increase of intracellular ROS occurs due to the dissipation of mitochondrial.[14]

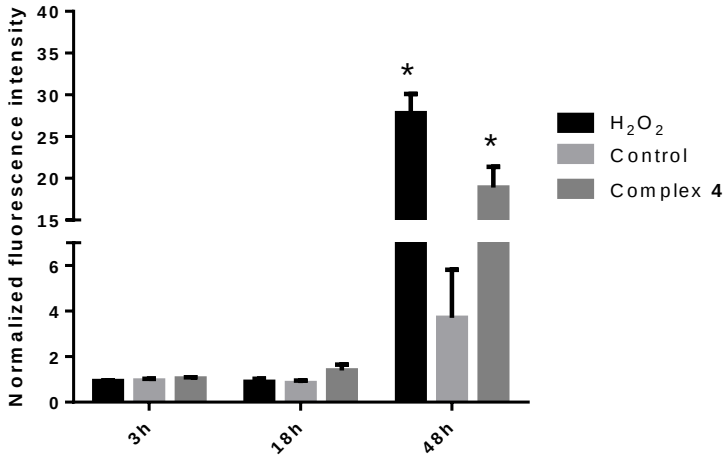

Figure 10. Reactive oxygen species (ROS) production in A2780 cells treated with compound **4**. A2780 cells were incubated for 3 h, 18 h and 48 h with RPMI 1640 medium supplemented with 10 % (v/v) fetal bovine serum and 25 μM Hydrogen peroxide (H_2O_2) (Black bars), 0.05 % (v/v) DMSO (light grey bars) and IC_{50} at 48 h of compound **4** (dark grey bars) and treated with H_2DCF-DA (2',7'-

dichlorodihydrofluorescein diacetate). ROS production was quantified in an Attune acoustic focusing cytometer (ThermoFisher Scientific) by the release of the green fluorescent compound DCF (excitation and emission wavelengths between 492-495 nm and 517-527 nm, respectively), in a reaction catalyzed by intracellular estereases. Values were normalized to the fluorescence of untreated cells. * p-value < 0.05 relative to the value of DMSO at the same time point.

These results suggest that, like other gold(I) compounds,[14] complex **4** induces intrinsic apoptosis. Accumulation of the complex in A2780 cells is higher for the first hours of incubation (Figure 6), when cells start to respond to the presence of the complex, resulting in mitochondrial hyperpolarization (Figure 9). The increased membrane polarization might be due to an increased metabolism induced by the complex. In fact, such response has been suggested by proteomic analysis of cisplatin-resistant A2780 cells exposed to gold(III) compounds, where an alteration of proteins involved in glycolytic pathway was observed.[64]

The hyperpolarization of the mitochondria is still observed after 18 h, when the apoptotic events have already started (Figures 7, 8). A slight increase of ROS is then observed (Figure 10). After 48 h, most cells are in apoptosis, resulting in a decrease of mitochondrial membrane potential and increase of ROS.

Conclusions

The synthesis of a series of mono- and dinuclear gold(I) complexes containing the same chromophoric unit (4-ethynylanile) and that differ on the phosphine located at the second coordination position has been successfully obtained by making react the [Au(4-ethynylaniline)]$_n$ polymer with the corresponding phosphane. The presence of carboxylic derived phosphanes and diphosphanes in *cis*-conformation avoids the formation of the products in pure form.

The presence of the same choromophoric unit in all complexes let us to perform a systematic analysis of the effect of phosphanes on the biological activity of gold(I) alkynyl complexes and retrieve some important conclusions: i) it is possible to modulate the selectivity of the treated tumor since mononuclear complexes are more cytotoxic against A2780 ovarian cells while dinuclear complexes are effective also against HCT116 colorectal cells; ii) the presence of PNaph$_3$ phosphine has a great selectivity against A2780 ovarian cells, having no cytotoxic effect neither on HCT116 colorectal cells nor on normal fibroblasts, making it a very interesting candidate of ovarian cancer with very low secondary effects; iii) the flexibility of the diphosphines has a direct influence on the biological activity, since the only dinuclear complex that do not present any denoted effect is that containing the higher rigid bridging ligand (dppa, complex **7**); iv) the results obtained for mitochondrial potential and ROS production in A2780 cells under the same experimental conditions suggest that, unlike auranofin, the increase of intracellular ROS could be due to an increased apoptosis, and not to thioredoxin reductase inhibition.

The results reported herein are of great importance to improve the understanding of the mechanism of activity of gold(I) complexes for future applications in ovarian cancer therapy.

Experimental Section

General procedures

All manipulations have been performed under prepurified N_2 using standard Schlenk techniques. All solvents have been distilled from appropriated drying agents. Commercial reagents 1,3,5-triaza-7-phosphatricyclo[3.3.1.13.7]decane (PTA, Aldrich 97%), 3,7-diacetyl-1,3,7-triaza-5-phosphabicyclo[3.3.1]nonane (DAPTA, Aldrich 97%), tri-1-naphthylphosphine ($PNaph_3$, Aldrich, 97%), triphenylphosphine (PPh_3, Aldrich, 97%), triethylphosphine (PEt_3, Strem Chemicals, 99%), bis(diphenylphosphino)acetylene (dppa, Aldrich, 98%), trans-1,2-bis(diphenylphosphino)ethylene (dppet, Aldrich, 97%), 1,3-bis(diphenylphosphino)propane (dppp, Aldrich 97%), and 4-ethynylaniline (Aldrich, 97%) were used as received. Literature methods were used to prepare AuCl(tht)[71] and 1,2-bis(diphenylphosphino)ethane (dppe).[72]

Physical measurements

Infrared spectra have been recorded on a FT-IR 520 Nicolet Spectrophotometer. ^{1}H NMR (δ(TMS) = 0.0 ppm) and ^{31}P{^{1}H} NMR (δ(85% H_3PO_4) = 0.0 ppm) spectra have been obtained on a Varian Mercury 400 and Bruker 400. ElectroSpray-Mass spectra (+) has been recorded on a Fisons VG Quatro spectrometer. Absorption spectra have been recorded on a Varian Cary 100 Bio UV- spectrophotometer and emission spectra on a Horiba-Jobin-Ybon SPEX Nanolog spectrofluorimeter. Elemental analyses of C, H and N were carried out at the CCiTUB in Barcelona.

X- ray crystal structure determination.

Single-crystal X-ray data for **4** and **10** was measured using a Rigaku SuperNova dual-source Oxford diffractometer[73] equipped with an Atlas detector using mirror-monochromated Cu-Kα (λ = 1.54184 Å) radiation. The data for **8** was measured using Rigaku SuperNova single-source diffractometer[73] fitted with an Atlas EoS CCD detector using mirror-monochromated Mo-*K*α (λ = 0.71073 Å) radiation. The data for **9** were measured on a Bruker-Nonius Kappa CCD diffractometer with an APEX-II CCD detector using graphite-monochromated Mo-Kα (λ = 0.71073 Å) radiation. The data collection and reduction for **4**, **8** and **10** collected using Rigaku instruments were performed using the program CrysAlisPro[73] and Gaussian face index absorption correction method[73] was applied. For the data obtained from Bruker Nonius Kappa diffractometer were performed

using the program COLLECT[74] and HKL DENZO and SCALEPACK.[75] The intensities for data collected using Bruker Nonius Kappa diffractometer were corrected for absorption using SADABS[76] with multi-scan absorption correction type method. All structures were solved with direct methods (SHELXS)[77] and refined by full-matrix least squares on F^2 using the OLEX2 software,[78] which utilizes the SHELXL-2013 module.[77] Constraints and restraints were used where appropriate for disordered models. Hirsfeld surface analysis details.[79]

X-ray crystallographic data for **4**, **8**, **9** and **10** are given in Supplementary information. CCDC-1844226 - 1844229 contains the supplementary crystallographic data for this paper. These data can be obtained free of charge from The Cambridge Crystallographic Data Centre via www.ccdc.cam.ac.uk/data_request/cif.

Cytotoxicity in human cell lines

Cell culture

Human ovarian carcinoma (A2780) and colorectal carcinoma (HCT116) were grown in RPMI 1640 and Dulbecco's modified Eagle's medium (DMEM), respectively (Invitrogen Corp., Grand Island, NY, USA) both supplemented with 10% fetal bovine serum and 1% antibiotic/antimycotic solution (Invitrogen Corp.) and maintained at 37 ºC in a humidified atmosphere of 5 % (v/v) CO_2.[80,81] Normal human primary fibroblasts were grown in the same conditions as HCT116 cell line, supplemented with 1 % MEM non-essential amino acids (Invitrogen Corp.).[82,83] All cell lines were purchase from ATCC (www.atcc.org).

Complexes exposure for dose-response curves

Cells were plated at 7500 cells/well in 96-well plates. Media was removed 24 h after platting and replaced with fresh media containing: 0.01 - 100 μM of each complex **2-10** or each ligand or 0.1 % (v/v) DMSO (vehicle control). Complexes and ligands solutions were prepared from a concentrated stock solution (in DMSO).

Viability assays

After 48 h of cell incubation in the presence or absence of the complexe**s** or each ligand, cell viability was evaluated with CellTiter 96® Aqueous One Solution Cell Proliferation Assay (Promega, Madison, WI, USA), using 3-(4,5-dimethylthiazol-2-yl)-5-(3-carboxymethoxyphenyl)-2-(4-sulfophenyl)-2H-tetrazolium, inner salt (MTS) as previously described.[83,84] In brief, this is a homogeneous, colorimetric method for

determining the number of viable cells in proliferation, cytotoxicity or chemosensitivity assays. The Cell Titer 96® Aqueous Assay is composed of solutions of MTS and an electron coupling reagent (phenazine ethosulfate, PES). MTS is bioreduced by cells into a formazan product that is soluble in tissue culture medium. The absorbance of the formazan product at 490 nm can be measured directly from 96-well assay plates without additional processing. The conversion of MTS into the aqueous soluble formazan product is accomplished by dehydrogenase enzymes found in metabolically active cells. The quantity of formazan product was measured in a Bio-Rad microplate reader Model 680 (Bio-Rad, Hercules, CA, USA) at 490 nm, as absorbance is directly proportional to the number of viable cells in culture.

Cellular uptake of complexes 2-10 by A2780 cells

To quantify the internalization of complexes **2-10** by A2780, $5x10^5$ cells were exposed to RPMI supplemented with a concentration of the complex at 10 x the respective IC_{50}, and incubated for 3 h at 37 ºC, 5 % (v/v) CO_2 and 99 % (v/v). The supernatant was then transferred to a new tube, cells were washed with phosphate buffer saline (PBS) that was added to the supernatant. Cells were then detached and pelleted by centrifugation at 500 *xg*, 5 min. The cell pellets were treated with *Acqua regia*, and the amount of Au quantified in each sample by Inductively Coupled Plasma-Atomic Emission Spectrometry (ICP-AES) - contracted service. The fraction of intracellular Au was obtained by dividing the Au concentration in the cell pellet by the sum of Au concentrations in cell pellet and Au concentration on the respective supernatant.

Complex 4 internalization in A2780 cells

Taking advantage of the fluorescence of complex **4** (excitation and emission wavelengths 310 nm and 410 nm, respectively in Tris-HCl 5 mM, pH 7.0, NaCl 50 mM), the internalization of the complex in A2780 cells was investigated by fluorescence microscopy. With that purpose, A2780 cells were seeded on a 24-well plate with a density of 1 x 10^5 cells/well and incubated for 24 h. The medium was replaced by fresh medium supplemented with 23 μM complex **4** (10 x IC_{50} complex **4** in A2780 cells), 0.05 % (v/v) DMSO (vector control) or non-supplemented (untreated cells). After 3 h, 6 h and 18 h, the medium was replaced by PBS and cells were immediately visualized on a Ti-U Eclipse inverted microscope (Nikon, Tokyo, Japan) with DAPI filter cube (Nikon) (excitation filter of 340-380 nm and barrier filter at 435-485 nm). Images were acquired

using NIS Elements Basic software (Nikon). The corrected total cell fluorescence (CTCF) was quantified for each cell using the formula: CTCF = integrated density – (area of cell x background mean fluorescence) and fluorescence intensity of DMSO and complex **4** treated samples was normalized with fluorescence intensity of untreated cells. Represented values correspond to the average and SEM of normalized fluorescence intensity observed in 20 cells analyzed in five random microscopic fields.

Apoptosis evaluation using Hoechst 33258 staining

A2780 cells were seeded in a 24 well plate containing a cover slip with 12 mm diameter, at a cell density of 37,500 cells/well. After 24 h, culture medium was replaced by fresh medium containing 2.3 μM complex **4** (IC_{50} of complex **4** in A2780 cells) or 0.05 % (v/v) DMSO (vehicle control) and incubated for 9 h at 37 ºC, 5 % (v/v) CO_2, 99 % (v/v) relative humidity. After washing 3 times with PBS, cells were fixed with 4 % (w/v) formaldehyde in PBS for 20 min in the dark, washed 3 times with PBS and stained for 15 min with 7.5 μg/mL Hoechst 33258 (LifeTechnologies). After wash 3 times with PBS coverslips containing the stained cells were placed on top of a glycerol drop, sealed. Cell nuclei were visualized on an AxioImager D2 microscope (Carl Zeiss, Oberkochen Germany), and acquired and processed using microscope respective software (ZEN Blue edition, 2011). Normal nuclei showed uniformly distributed chromatin; condensed or fragmented chromatin was visualized on the nuclei and/or when apoptotic bodies were imaged indicated apoptotic cells. Values correspond to the average and SEM of apoptotic events observed in five random microscopic fields containing 20 nuclei each.

Western-Blot for BAX and BCL-2 quantification

A2780 cells were plated on T-flasks with 25 cm^2 with a cell density of 7.5 x 10^5 cells. After 24 h incubation to allow cells to adhere, the medium was replaced by fresh medium supplemented with 2.3 μM complex **4** (IC_{50} complex **4** in A2780 cells) or 0.05 % (v/v) DMSO (vector control) and incubated at 37 ºC, 5 % (v/v) CO_2 and 99 % (v/v) relative humidity for 3 h, 18 h or 48 h. Cell monolayer was washed 3 times with PBS and cells were detached using a cell scraper in 2 mL PBS. Cells were pelleted using a centrifugation 500 *xg* 5 min and following procedure was identical to a previously described,[85] with the exception that a PVDF membrane (GE Healthcare) was used and signal acquisition was obtained in a Hyperfilm ECL (GE Healthcare). The quantification of protein band

intensity was performed using FIJI software.[86] To calculate the percentage of BAX and BCL-2 the band intensity was first normalized to β-actin values and then to the value of the sample incubated for 3 h with DMSO.

Mitochondrial membrane potential

The evaluation of mitochondrial membrane potential was based on measurement of JC-1 dye fluorescence. Briefly, 37500 A2780 cells were seeded on a 24 well plate with a cover sleep and let to adhere for 24 h. The medium was then replaced with fresh medium supplemented with 2.3 μM complex **4** (IC_{50} complex **4** in A2780 cells), 0.05 % (v/v) DMSO (vector control) and with non-supplemented medium (untreated cells). After 3 h, 18 h and 48 h, cells were stained with JC-1 dye (Life Technologies, ThermoFisher Scientific, Waltham, Massachusetts, EUA) according to manufacturer's instructions. After 20 min incubation at 37 ºC, 5 % (v/v) CO_2 and 99 % (v/v) relative humidity, coverslips were placed on a microscopic slide and immediately visualized in an AxioImager D2 microscope and respective software. The JC-1 is a green fluorescent dye (emission fluorescence 529 nm) that forms red fluorescent aggregates (emission fluorescence 590 nm) when accumulates in the mitochondria with higher membrane potential.[87] Five random microscopic fields were analyzed using in the same field, autoexposure for brigthfield image acquisition, 150 ms exposure for image acquisition of JC-1 dye in aggregate conformation, using rhodamine fluorophore settings (excitation and emission wavelength 540 nm and 570 nm, respectively) and 150 ms exposure for image acquisition of the monomer conformation, using FITC settings (excitation and emission wavelength 485 nm and 535 nm, respectively). The relative fluorescent cell intensity of each cell was measured using FIJI software[86] and CTCF was quantified for each JC-1 conformation. After calculating the monomer/aggregate CTCF ratio, values were normalized with ratios obtained for untreated cells.

Quantification of Reactive Oxygen Species (ROS)

A2780 cells were seeded in a 6 well plate in a density of 1 x 10^5 cells/well. After 24 h incubation, medium was discarded and replaced with fresh medium supplemented with 2.3 μM complex **4** (IC_{50} complex **4** in A2780 cells), 0.05 % (v/v) DMSO (vector control), 25 μM H_2O_2 (positive control for ROS induction), and with non-supplemented medium (untreated cells). After 3 h, 18 h and 48 h incubation, cells were detached, centrifuged 5

min at 500 *xg*, washed 2 times with PBS and resuspended in a pre-warmed solution of 10 μM H_2DCF-DA (LifeTechnologies) in PBS. H_2DCF-DA (2',7'-dichlorodihydrofluorescein diacetate) is a cell permeant non-fluorescent reduced form of fluorescein that after cleavage of acetate groups by intracellular estereases and oxidation, forms green fluorescent DCF (2',7'-dichlorofluorescein) (excitation and emission wavelengths between 492-495 nm and 517-527 nm, respectively). Data was acquired using an Attune acoustic focusing cytometer (ThermoFisher Scientific) and respective software (Attune Cytometric Software, vs 2.1). Data was represented as the mean fluorescence intensity of each sample normalized to the fluorescence intensity of untreated cells.

Statistical analysis

All data were expressed as mean ± SEM from at least three independent experiments. Statistical significance was evaluated using the Student's t-test; $p < 0.05$ was considered statistically significant.

Synthesis and characterization

***Synthesis of [Au(C≡C-$C_6H_4NH_2$)]$_n$* (1)**

Complex **1** was prepared by introducing slight modifications of the procedure previously reported on the literature.[29] NEt_3 (0.54 ml, 3.87 mmol) and AuCl(tht) (0.70 g, 2.19 mmol) were added into a stirring solution of 4-ethynylaniline (0.26 g, 2.20 mmol) in dichloromethane (35 ml) under N_2 atmosphere at room temperature. After stirring for 30 min the resulting orange suspension was filtered, washed with dichloromethane (3×15 ml) and dried under vacuum. Yield: 92% (0.63 g). IR (KBr, cm^{-1}): 3363 s, 3202 s (N-H); 1994 w (C≡C).

***Synthesis of [Au(4-ethynylaniline)(PTA)]* (2)**

Solid PTA (50.5 mg, 0.32 mmol) was added into a stirring suspension of **1** (0.10 g, 0.32 mmol) in dichloromethane (20 ml) under N_2 atmosphere at room temperature. The reaction mixture turned white after 10 min of stirring. The resulting suspension was concentrated in half volume after 2 h of stirring and hexane (17 ml) was added to favor precipitation. The resulting white solid was filtrated, washed with hexane (3 ml) and dried under vacuum. Purification of the solid was performed by stirring in dichloromethane:methanol:acetonitrile (10:3:3) mixture. The suspension was

concentrated and precipitated with hexane (10 ml) to obtain a white solid in 63% yield (95.3 mg). ^{1}H NMR (400 MHz, $CDCl_3$, ppm): δ_H 7.26 (dt, J_1 = 8.4, J_2 = 2.4 Hz, 2H, H_β), 6.55 (dt, J_1 = 8.4, J_2 = 2.4 Hz, 2H, H_α), 4.54 (d, J = 13.2 Hz, 3H, N-CH_2-N), 4.47 (d, J=13.2 Hz, 3H, N-CH_2-N), 4.22 (s, 6H, N-CH_2-P), 3.68 (br, 2H, NH_2). ^{31}P{^{1}H} NMR ($CDCl_3$, 161.9 MHz, ppm): -49.4. IR (KBr, cm^{-1}): 3424 s, 3355 s (N-H); 2102 w (C≡C). ESI-MS *m/z* 471.095 ([M+H]$^+$, calc.: 471.094). Anal. Calc. for $C_{14}H_{18}AuN_4P$ C 35.76, H 3.86, N 11.91; found C 35.82, H 3.78, N 11.98.

***Synthesis of [Au(4-ethynylaniline)(DAPTA)]* (3)**

Solid DAPTA (73.7 mg, 0.32 mmol) was added into a stirring suspension of **1** (0.10 g, 0.32 mmol) in dichloromethane (20 ml) under N_2 atmosphere at room temperature. The reaction mixture turned clear yellow after stirring for 10 min. The resulting yellow suspension was concentrated after 2 h of stirring and hexane (17 ml) was added to favor the precipitation. The yellow product was filtrated, washed with hexane (6 ml), dried under vacuum and recrystallized with acetonitrile (10 ml)/ diethylether (7 ml) to give a yellow solid in 51% yield (88.7 mg). ^{1}H NMR (400 MHz, $CDCl_3$, ppm): 7.27 (dt, J_1 = 7.7, J_2 = 2.7 Hz, 2H, H_β), 6.56 (dt, J_1 = 8.5, J_2 = 2.4 Hz, 2H, H_α), 5.79 (d, J = 22.3 Hz, 1H, N-CH_2-N), 5.60 (dd, J_1 = 15.6, J_2 = 7.0, 1H, P-CH_2-N), 4.95 (d, J = 14.3 Hz, 1H, N-CH_2-N), 4.56–4.64 (m, 2H, N-CH_2-N and P-CH_2-N), 4.09 (dt, J_1 =15.9, J_2 = 3.0 Hz, 1H, P-CH_2-N), 4.04 (d, J = 14.8 Hz, 1H, N-CH_2-N), 3.82 (s, 2H, P-CH_2-N), 3.71 (s, 2H, C-NH_2), 3.49 (dt, J_1 =16.0, J_2 = 4.0 Hz, 1H, P-CH_2-N), 2.10 (d, J = 2.2 Hz, 6H, CO-CH_3) ppm. ^{31}P{^{1}H} NMR ($CDCl_3$, 161.9 MHz, ppm): -22.5 (s, 1P) ppm. IR (KBr, cm^{-1}): 3456 s, 3353 s (N-H); 2099 w (C≡C). ESI-MS *m/z* 543.115 ([M+H]$^+$, calc.: 543.115). Anal. Calc. for $C_{17}H_{22}AuN_4O_2P$ C 37.65, H 4.09, N 10.33; found C 37.51, H 4.15, N 10.38.

***Synthesis of [Au(4-ethynylaniline)(tri-1-naphthylphosphine)]* (4)**

Solid tri-1-naphthylphosphine (0.13 g, 0.32 mmol) was added at once into a stirring suspension of **1** (0.10 g, 0.32 mmol) in dichloromethane (20 ml) under N_2 atmosphere at rt. The solution turned pale yellow and turbid after 10 min of stirring. The resulting suspension was concentrated to the half after stirring for 2 h, and hexane (15 ml) was added. The pale-yellow suspension was filtrated, washed with hexane (5 ml) and dried in vacuum. The crude product was purified by stirring with acetonitrile and adding diethylether to precipitate a pale-yellow product in 56% yield (0.13 g). ^{1}H NMR (400 MHz, $CDCl_3$, ppm): 8.82 (d, J = 8.0 Hz, 3H, H_{Naph}), 8.02 (d, J = 8.0 Hz, 3H, H_{Naph}), 7.95

(d, J = 8.0 Hz, 3H, H_{Naph}), 7.57 (td, J = 8.0 Hz, J_2 = 4.0 Hz, 3H, H_{Naph}), 7.51 (td, J_1 = 8.0 Hz, J_2 = 4.0 Hz, 3H, $_{Naph}$, 7.34-7.28 (m, 6H, H_{Naph}), 7.22 (d, J = 8.4, 2H, H_β), 6.50 (d, J = 8.4, 2H, H_α), 3.61 (s, 2H, C-NH_2) ppm. $^{31}P\{^1H\}$ NMR ($CDCl_3$, 161.9 MHz): 22.3. IR (KBr, cm^{-1}): 3451 s, 3354 s (N-H); 2107 w (C≡C). ESI-MS *m/z* 726.155 ($[M+H]^+$, calc.: 726.155). Anal Calc for $C_{38}H_{27}AuNP$ C 62.90, H 3.75, N 1.93; found C 62.79, H 3.74, N 1.91.

Synthesis of [Au(4-ethynylaniline)(PPh$_3$)] **(5)**

The synthesis of **5** was carried out following the procedure previously reported in the literature.[25] IR (KBr, cm^{-1}): 3451 s, 3321 s (N-H); 2104 w (C≡C). ^1H NMR (400 MHz, $CDCl_3$): 7.61-7.39 (m, 15H, Ph), 7.33 (d, J = 8.0 Hz, 2H, H_β), 6.56 (d, J = 8.0 Hz, 2H, H_α), 3.67 (s, 2H, NH_2) ppm. $^{31}P\{^1H\}$ NMR (400 MHz, $CDCl_3$): 42.5. ESI-MS *m/z* 576.115 ($[M+H^+]$, calc.: 576.110); 1034.164 ($[M+AuPPh_3]^+$, calc.:1034.165. Anal. Calc for $C_{26}H_{21}AuNP$ C 54.27, H 3.68, N 2.43; found C 54.12, H 3.89, N 2.54.

Synthesis of [Au(4-ethynylaniline)(PEt$_3$)] **(6)**

The complex was synthesised with the same method as **5** but using 0.16 mmol of reagents instead of 0.32. Yield: 30 mg (43 %). IR (KBr, cm^{-1}): 3412 s (N-H); 2098 w (C≡C). ^1H NMR (400 MHz, $CDCl_3$, ppm): 7.30 (d, J = 8.0 Hz, 2H, H_β), 6.54 (d, J = 8.0 Hz, 2H, H_α), 3.66 (s, 2H, NH_2), 1.86-1.73 (m, 6H, CH_2), 1.27-1.13 (m, 9H, CH_3). $^{31}P\{^1H\}$ NMR (161.9 MHz, $CDCl_3$, ppm): 38.1. ESI-MS *m/z* 432.115 ($[M+H^+]$, Calc.: 432.110); 454.096 ($[M+Na^+]$, Calc.: 454.097). Anal. Calc for $C_{14}H_{21}AuNP$ C 38.99, H 4.91, N 3.25; found C 38.82, H 4.87, N 3.38.

Synthesis of [Au(4-ethynylaniline)]$_2$μ-(dppa) **(7)**

Solid dppa (63 mg, 0.16 mmol) was added to a steering suspension of **1** (0.10 g, 0.32 mmol) in dichloromethane under N_2 atmosphere at room temperature. After 40 min of stirring, the reaction mixture was concentrated to the half and hexane (20 ml) was added to precipitate the yellow solid that was dried and obtained in 72% yield (118 mg). IR (KBr, cm^{-1}): 3463 s, 3331 s (N-H); 2108 w (C≡C).. ^1H NMR (400 MHz, $CDCl_3$, ppm): 7.77-7.36 (m, 20H, Ph), 7.33 (d, J = 8.4 Hz, 4H, H_β), 6.57 (d, J = 8.4 Hz, 4H, H_α), 3.67 (s, 4H, NH_2). $^{31}P\{^1H\}$ NMR (161.9 MHz, $CDCl_3$, ppm): 16.7. ESI-MS *m/z* 1021.136 ($[M+H^+]$, Calc.: 1021.137); 985.173 ($[M + H^+ - Ph + CH_3CN]^+$, Calc.: 985.170). Anal Calc for $C_{42}H_{32}Au_2N_2P_2$ C 49.43, H 3.16, N 2.74; found C 49.38, H 3.20, N 2.79.

Synthesis of [Au(4-ethynylaniline)]$_2$μ-(dppet) **(8)**

Complex **8** was synthesized following the same experimental procedure reported for **7** but using dppet instead of dppa. A pale yellow solid was obtained in 20% yield (32 mg). IR (KBr, cm^{-1}): 3450 s, 3333s (N-H); 2106 w (C≡C). ^{1}H NMR (400 MHz, $CDCl_3$, ppm): 7.65-7.42 (m, 22H, Ph + P-C*H*=C*H*-P), 7.30 (d, *J* = 8.0 Hz, 4H, H_β), 6.55 (d, *J* = 8.0 Hz, 4H, H_α), 3.69 (s, 4H, N*H*$_2$). ^{31}P{^{1}H} NMR (161.9 MHz, $CDCl_3$, ppm): 39.1. ESI-MS *m/z* 1023.159 ([M+H$^+$], Calc.: 1023.153); 989.205 ([M-2xNH_2), Calc.: 989.200); 906.101 ([M-ethynylaniline)]$^+$, Calc.: 906.103). Anal Calc for $C_{42}H_{34}Au_2N_2P_2$ C 49.33, H 3.35, N 2.74; found 49.24, H 3.31, N 2.70.

Synthesis of [Au(4-ethynylaniline)]$_2$μ-(dppe) **(9)**

Complex **9** was synthesized following the same experimental procedure reported for **7** but using dppe instead of dppa. A yellow solid was obtained in 76% yield (125 mg). IR (KBr, cm^{-1}): 3455 s, 3343 s (N-H); 2104 w (C≡C). ^{1}H NMR (400 MHz, $CDCl_3$, ppm): 7.72-7.13 (m, 24H, Ph + H_β), 6.58 (d, *J* = 8.0 Hz, 4H, H_α), 3.70 (s, 4H, N*H*$_2$), 2.47 (s br, 4H, P-C*H*$_2$). ^{31}P{^{1}H} NMR (161.9 MHz, $CDCl_3$, ppm): 21.1. ESI-MS *m/z* 1025.174 ([M+H$^+$], Calc.: 1025.170). Anal Calc for $C_{42}H_{36}Au_2N_2P_2$ C 49.23, H 3.54, N 2.73; found C 49.02, H 3.53, N 2.75.

Synthesis of [Au(4-ethynylaniline)]$_2$(dppp) **(10)**

Complex **10** was synthesized following the same experimental procedure reported for **7** but using dppp instead of dppa. A pale yellow solid was obtained in 54% yield (89 mg). IR (KBr, cm^{-1}): 3431 s, 3339 s (N-H); 2106 w (C≡C). ^{1}H NMR (400 MHz, $CDCl_3$, ppm): 7.69-7.30 (m, 20H, Ph), 7.25 (*J* = 8.0 Hz, 4H, H_β), 6.50 (d, *J* = 8.0 Hz, 4H, H_α), 3.62 (s, 4H, N*H*$_2$), 2.80-266 (m, 4 H, P-C*H*$_2$-CH$_2$-C*H*$_2$-P), 1.98-1.78 (m, 2 H, P-CH$_2$-C*H*$_2$-CH$_2$-P). ^{31}P{^{1}H} NMR (161.9 MHz, $CDCl_3$, ppm): 35.5. ESI-MS *m/z* 1061.174 ([M+Na$^+$]$^+$, Calc. 1061.174); 1039.192 ([M+H$^+$]$^+$, Calc.: 1038.194); 1021.2657; 520.098 ([M+2H$^+$]$^{2+}$, Calc.: 520.098). Anal Calc for $C_{43}H_{38}Au_2N_2P_2$ C 49.72, H 3.69, N 2.70; found 49.61, H 3.67, N 2.73.

Synthesis of potassium 4-(diphenylphosphanyl)benzoate **(11).** 4-(Diphenylphosphanyl)benzoic acid (70.9 mg, 0.23 mmol) was treated with KOH (16.1 mg, 0.29 mmol) in methanol under N_2 atmosphere. After stirring for 1.5 h at room temperature the clear solution was concentrated until dryness. Diethylether (10 ml) was added and the resulting suspension was sonicated for 10 min, filtered and dried under

vacuum to give $(C_6H_5)_2PC_6H_4CO_2K$ in 84% yield (66.7 mg). ^{1}H NMR (400 MHz, $CDCl_3$, ppm): 7.47 (d, *J* = 7.6 Hz, 2H, HOOC-C-C*H*), 7.11–7.17 (m, 10H, C-*H*), 6.86 (t, *J* = 7.5 Hz, 2H, PC-C*H*) ppm. $^{31}P\{^1H\}$ NMR (161.9 MHz, $CDCl_3$, ppm): -6.2. IR (KBr, ν_{max} cm^{-1}): ν(COOK) 1587, 1394. ESI-MS *m/z* 305.07 ($[M-K]^-$, calc.: 305.07).

Supporting Information

Schemes of the reactions for the formation of the complexes; NMR data; X-ray crystal structure and collection data and main distances and angles; absorption and emission spectra; Cytotoxicity of the ligands at 48 h in A2780 cell line, HCT116 cell line and normal human fibroblasts.

Acknowledgements

The authors are grateful to the Ministry of Economy, Industry and Competitiveness of Spain (AEI/FEDER, UE Project CTQ2016-76120-P). This work was also supported by the Associated Laboratory for Sustainable Chemistry, Clean Processes and Technologies, LAQV, which is financed by national funds from FCT/MEC (UID/QUI/50006/2013) and co-financed by the ERDF under the PT2020 Partnership Agreement (POCI-01-0145-FEDER-007265) and by the Unidade de Ciências Biomoleculares Aplicadas-UCIBIO which is financed by national funds from FCT/MEC (UID/Multi/04378/2013) and co-financed by the ERDF under the PT2020 Partnership Agreement (POCI-01-0145-FEDER-007728). COST Action CM1402 is also acknowledged. N.S. is also indebted to Erasmus exchange mobility Program. We also would like to thank Ms. Andrea Pinto and Mr. Oussama Kheireedine Nehar for the help in some of the syntheses performed. The University of Jyväskylä (KR) and The Academy of Finland (RP, grant no. 298817) are kindly acknowledged for financial support.

References

[1] L. Kelland, *Nat. Rev. Cancer* **2007**, *7*, 573.

[2] I. Ott, *Coord. Chem. Rev.* **2009**, *253*, 1670.

[3] J.C. Lima, L. Rodríguez, *Anticancer Agents Med. Chem*. **2011**, *11*, 921.

[4] C. Nardon, G. Boscutti, D. Fregona, *Anticancer Res.* **2014**, *34*, 487.

[5] T. Zou, C.T. Lum, C.N. Lok, J.J. Zhang, C.M. Che, *Chem. Soc. Rev*. **2015**, *44*, 8786.

[6] T. Traut-Johnstone, S. Kanyanda, F.H. Kriel, T Viljoen, P.D.R. Kotze, W.E. van Zyl, J. Coates, D.J.G. Rees, M. Meyer, R. Hewer, D.B.G.Williams, *J. Inorg. Biochem*. **2015**, *145*, 108.

[7] S.P. Fricker *Anticancer Agents Med. Chem.* **2011**, *11*, 940.

[8] C. Gabbiani, L. Messori, *Anticancer Agents Med. Chem.* **2011**, *11*, 929.

[9] A. Casini, M.A. Cinellu, G. Minghetti, C. Gabbiani, M. Coronnello, E.Mini, L. Messori, *J. Med. Chem.* **2006**, *49*, 5524.

[10] B. Bertrand, L. Stefan, M. Pirrotta, D. Monchaud, E. Bodio, P. Richard, P. Le Gendre, E. Warmerdam, M.H. de Jager, G.M.M. Groothuis, M. Picquet, A. Casini, *Inorg. Chem.* **2014**, *53*, 2296

[11] M. J. McKeage, L. Mahara, S. J. Berners-Price, *Coord. Chem. Rev*. **2002**, *232*, 127.

[12] S. Schafer, W. Frey, A.S.K. Hashmi, V. Cmrecki, A. Luquin, M. Laguna, *Polyhedron* **2010**, *29*, 1925.

[13] A. Meyer, C. P. Bagowski, M. Kokoschka, M. Stefanopoulou, H. Alborzinia, S. Can, D. H. Vlecken, W. S. Sheldrick, S. Wölfl, I. Ott. *Angew. Chem., Int. Ed.* **2012**, *51*, 8895.

[14] P.J. Barnard, S.J. Berners-Price. *Coord. Chem. Rev.* **2007**. *251*, 1889.

[15] M. Porchia, M. Pellei, M. Marinelli, F. Tisato, F. D. Bello, C. Santini. *Eur. J. Med. Chem.* **2018**, *146*, 709.

[16] A. Casini, L. Messori. *Curr. Top. Med. Chem.* **2011**, *11*, 2647.

[17] T. Zou, C. Tung Lum, C.-N. Lok, J.-J. Zhang, C.-M. Che. *Chem. Soc. Rev.* **2015**, *44*, 8786.

[18] a) A.J. Moro, B. Rome, E. Aguiló, J. Arcau, R. Puttreddy, K. Rissanen, J.C. Lima, L. Rodríguez, *Org. Biomol. Chem.* **2015**, *13*, 2026; b) M. Ferrer, A. Gutiérrez, L. Rodríguez, O. Rossell, E. Ruiz, M. Engeser, Y. Lorenz, R. Schilling, P. Gómez-Sal, A. Martín, *Organometallics* **2012**, *31*, 1533; c) E. Aguiló, A.J. Moro, R. Gavara, I. Alfonso, Y. Pérez, F. Zaccaria, C. Fonseca Guerra, M. Malfois, C. Baucells, M. Ferrer, J.C. Lima, L.

Rodríguez, *Inorg. Chem*. **2018**, *57*, 1017; d) D. Gallenkamp, T. Porsch, A. Molter, E.R.T. Tiekink, F. Mohr, *J. Organomet. Chem.* **2009**, *694*, 2380.

[19] a) P. de Frémont, N. Marion, S.P. Nolan, *J. Organomet. Chem*. **2009**, 694, 551; b) A. S.K. Hashmi, C. Lothschütz, K. Graf, T. Häffner, A. Schuster, F. Rominger, *Adv. Synth. Catal*. **2011**, *353*, 1407; c) A.S.K. Hashmi, C. Lothschütz, C. Bçhling, T. Hengst, C. Hubbert, F. Rominger, *Adv. Synth. Catal*. **2010**, *352*, 3001; d) T. Wurm, F. Mulks, C.R.N. Böhling, D. Riedel, P. Zargaran, M. Rudolph, F. Rominger, A.S.K. Hashmi *Organometallics* **2016**, *35*, 1070; e) D. Riedel, T. Wurm, K. Graf, M. Rudolph, F. Rominger, A.S.K. Hashmi, *Adv. Synth. Catal*. **2015**, *357*, 1515; f) A.S.K. Hashmi, D. Riedel, M. Rudolph, F. Rominger, T. Oeser, *Chem. Eur. J.* **2012**, *18*, 3827.

[20] a) C. Khin, A.S.K. Hashmi, F. Rominger, *Eur. J. Inorg. Chem.* **2010**, 1063; b) G. Dyker, *Angew Chem. Int. Ed*. **2000**, *39*, 4237; c) A.S.K. Hashmi, *Chem. Rev.* **2007**, *107*, 3180; d) L. Zhang, *Acc. Chem. Res.* **2014**, *47*, 877; e) D. Pflästerer, A.S.K. Hashmi, *Chem. Soc. Rev*. **2016**, *45*, 1331.

[21] S.N. Britvin, A. Lotnyk. *J. Am. Chem. Soc.* **2015**, *137*, 5526.

[22] T.S. Reddy, S.H. Privér, N. Mirzadeh, S.K. Bhargava. *J. Inorg. Biochem*. **2017**, *175*, 1.

[23] J.C. Lima, L. Rodríguez. *Chem. Soc. Rev.* **2011**, *40*, 5442.

[24] M. Dalmases, E. Aguiló, J. Llorca, L. Rodríguez, A. Figuerola. *Chem. Phys. Chem.* **2016**, *17*, 2190.

[25] E. Aguiló, L. Soler, A. Casanovas, A.J. Moro, J.C. Lima, L. Rodríguez, J. Llorca. *Chem. Cat. Chem*. **2017**, *9*, 3289.

[26] J. Gil-Rubio, J. Vicente. *Chem. Eur. J.* **2018**, *24*, 32.

[27] A. Pinto, N. Svahn, J.C. Lima, L. Rodríguez. *Dalton Trans*. **2017**, *46*, 11125

[28] E. Vergara, E. Cerrada, A. Casini, O. Zava, M. Laguna, P. J. Dyson, *Organometallics* **2010**, *29*, 2596.

[29] G. Hogarth, M.M. Álvarez-Falcón. *Inorg. Chim. Acta* **2005**, *358*, 1386

[30] E. Schuh, S. M. Valiahdi, M. A. Jakupec, B. K. Keppler, P. Chiba, F. Mohr. *Dalton Trans.* **2009**, 10841.

[31] C.-H. Chui, R.-M. Wong, R. Gambari, G. Y.-M. Cheng, M. C.-W. Yuen, K.-W. Chan, S.-W. Tong, F.-Y. Lau, P. B.-S. Lai, K.-H. Lam, C.-L. Ho, C.-W. Kan, K. S.-Y. Leung, W.-Y. Wong. *Bioorg. Med. Chem*. **2009**, *17*, 7872.

[32] C. Wetzel, P.C. Kunz, M.U. Kassack, A. Hamacher, P. Böhler, W. Watjen, I. Ott, R. Rubbiani, B. Spinglere. *Dalton Trans*. **2011**, *40*, 9212.

[33] A. Meyer, A. Gutiérrez, I. Ott, L. Rodríguez. *Inorg. Chim. Acta* **2013**, *398*, 72.

[34] J. Arcau, V. Andermark, E. Aguiló, A. Gandioso, A. Moro, M. Cetina, J.C. Lima, K. Rissanen, I. Ott, L. Rodríguez. *Dalton Trans*. **2014**, *43*, 4426.

[35] V. Andermark, K. Göke, M. Kokoschka, M.A. Abu el Maaty, C. Tung Lumg, T. Zou, R. Wai-Yin Sun, E. Aguiló, L. Oehninger, L. Rodríguez, H. Bunjes, S. Wölfl, C.-M. Che, I. Ott. *J. Inorg. Biochem*. **2016**, *160*, 140.

[36] R. Gavara, E. Aguiló, J. Schur, J. Llorca, I. Ott, L. Rodríguez. *Inorg. Chim. Acta* **2016**, *446*, 189.

[37] C. Sánchez-de-Diego, I. Mármol, R. Pérez, S. Gascón, M.J. Rodriguez-Yoldi, E. Cerrada. *J. Inorg. Biochem.* **2017**, *166*, 108.

[38] I. Mármol, M. Virumbrales-Muñoz, J. Quero, C. Sánchez-de-Diego, L. Fernández, I. Ochoa, E. Cerrada, M.J. Rodríguez Yoldi. *J. Inorg. Biochem.* **2017**, *176*, 123.

[39] E. Aguiló, R. Gavara, C. Baucells, M. Guitart, J.C. Lima, J. Llorca, L. Rodríguez, *Dalton Trans*. **2016**, *45*, 7328.

[40] R. Gavara, J. Llorca, J.C. Lima, L. Rodríguez. *Chem. Commun*. **2013**, *49*, 72.

[41] E. Aguiló, R. Gavara, J.C. Lima, J. Llorca, L. Rodríguez. *J. Mater. Chem. C* **2013**, *1*, 5538.

[42] S.K. Schneider, W.A. Herrmann, E. Herdtweck, *Z. Anorg. Allg. Chemie* **2003**, *629*, 2363.

[43] D.-A. Rosca, J.A. Wright, M. Bochmann. *Dalton. Trans*. **2015**, *44*, 20785.

[44] F. Mohr, M.C. Jennings, R.J. Puddephatt. *Angew. Chem. Int. Ed*. **2004**, *43*, 969.

[45] L.L. Shevchenko. *Russ. Chem. Rev*. **1963**, *32*, 201.

[46] A.S.K. Hashmi, *Acc. Chem. Res.* **2014**, *47*, 864.

[47] H. Schmidbaur, A. Schier, *Chem. Soc. Rev*. **2012**, *41*, 370.

[48] M. A. Spackman, P. G.Byrom, *Chem. Phys. Lett*. **1997**, *267*, 21.

[49] J. J. McKinnon, M. A. Spackman, A. S. Mitchell, *Acta Cryst* **2004**, *B60*, 627.

[50] F. L. Hirshfeld, *Theoret. Chim. Acta* **1977**, *44*, 129.

[51] Daniel T. Walters, Kellie R. England, Kamran B. Ghiassi, Fikerete Z. Semma, Marilyn M. Olmstead, Alan L. Balch *Polyhedron* **2016**, *117*, 535.

[52] S. Onaka, M. Yaguchi, R. Yamauchi, T. Ozeki, M. Ito, T. Sunahara, Y. Sugiura, M. Shiotsuka, K. Nunokawa, M. Horibe, K. Okazaki, A. Iida, H. Chiba, K. Inoue, H. Imai, K. Sako, *J. Organomet. Chem.* **2005**, *690*, 57.

[53] W. J. Wolf, M. S. Winston, F. D. Toste *Nature Chem.* **2014**, *6*, 159.

[54] T. J. Burchell, D. J. Eisler, M. C. Jennings, R. J. Puddephatt, *Chem. Commun.* **2003**, 2228.

[55] S. Han, Y. Y. Yoon, O.-S. Jung, Y.-A Lee, *Chem. Commun.* **2011**, *47*, 10689.

[56] N. C. Habermehl, D. J. Eisler, C. W. Kirby, N. L.-S. Yue, R. J. Puddephatt, *Organometallics* **2006**, *25*, 2921.

[57] V. Cámara, N. Masciocchi, J. Gil- Rubio, J. Vicente, *Chem. Eur. J*. **2014**, *20*, 1389.

[58] O. Crespo, C. Díez-Gil, M. C. Gimeno, P. G. Jones, A. Laguna, I. Ospino, J. Tapias, M. D. Villacampa, R. Visbal, *DaltonTrans.* **2013**, *42*, 8298.

[59] M. Ferrer, A. Gutiérrez, L. Rodríguez, O. Rossell, J.C. Lima, M. Font-Bardia, X. Solans, *Eur. J. Inorg. Chem.* **2008**, 2899.

[60] X.-L. Li, M. Tan, K.-J. Zhang, B. Yang, J. Chen, Y.-B. Ai, *Inorg. Chem.* **2012**, *51*, 109.

[61] L. Rodríguez, M. Ferrer, R. Crehuet, J. Anglada J.C. Lima. *Inorg. Chem.*, **2012**, *51*, 7636.

[62] G. Perichet, R. Chapelon, B. Pouyet, *J. Photochem.* **1980**, *13*, 67.

[63] E. Vergara, A. Casini, F. Sorrentino, O. Zava, E. Cerrada, M.P. Rigobello, A. Bindoli, M. Laguna, P.J. Dyson. *Chem. Med. Chem*. **2010**, *5*, 96.

[64] F. Guidi, I. Landini, M. Puglia, F. Magherini, C. Gabbiani, M.A. Cinellu, S. Nobili, T. Fiaschi, L. Bini, E. Mini, L. Messori, A. Modesti. *Metallomics*. **2012**, *4*, 307.

[65] I. Landini, A. Lapucci, A. Pratesi, L. Massai, C. Napoli, G. Perrone, P. Pinzani, L. Messori, E. Mini, S. Nobili. *Oncotarget* **2017**, *8*, 96062.

[66] F. Tisato, L. Crociani, M. Porchia, P. Di Bernardo, F. Endizzi, C. Santini, R. Seraglia. *Rapid Commum Mass Sepctrom.* **2013**, *27*, 2019.

[67] E.A. Prokhorova, A.V. Zamaraev, G.S. Kopeina, B. Zhivotovsky, I.N. Lavrik. *Cell. Mol. Life Sci*. **2015**, *72*, 4593.

[68] A.M. Hata, J.A. Engelman, A.C. Faber. *Cancer Discov*. **2015**, *5*, 475.

[69] O. Kepp, L. Galuzzi, M. Lipinski, J. Yuan, G. Kroemer. *Nat. Rev. Drug Discov*. **2011**, *10*, 221.

[70] M. Reers, T.W. Smith, L.B. Chen. *Biochem*. **1991**, *30*, 4480.

[71] R. Usón, A. Laguna. *Organomet. Synth.* **1986**, *3*, 322.

[72] W. Hewertson, H.R. Watson. *J. Chem. Soc*., **1962**, 1490.

[73] *Rigaku Oxford Diffraction 2017*, *CrysAlisPro* Version 1.171.38.43.

[74] Bruker AXS BV, Madison, WI, USA; 1997–2004

[75] Z. Otwinowski, W. Minor, *Methods Enzymol.* **1997**, *276*, 307.

[76] R. H. Blessing, *J. Appl. Cryst.* **1997**, *30*, 421.

[77] G. M. Sheldrick, *Acta Cryst*. **2015**, *C71*, 3.

[78] O. V. Dolomanov, L. J. Bourhis, R. J. Gildea, J. A. K. Howard, H. J. Puschmann, *Appl. Cryst.* **2009**, *42*, 339.

[79] M. A. Spackman, D. Jayatilaka, *CrystEngComm*, **2009**, *11*, 19.

[80] A. Silva, D. Luis, S. Santos, J. Silva, A.S. Mendo, L. Coito, T.F. Silva, M.F. da Silva, L.M. Martins, A.J. Pombeiro, P.M. Borralho, C.M. Rodrigues, M.G. Cabral, P.A. Videira, C. Monteiro, A.R. Fernandes. *Drug Metabol. Drug Interact*. **2013**, *28*, 167.

[81] O.A. Lenis-Rojas, A.R. Fernandes, C. Rodrigues, P.V. Baptista, F.M. Marques, D. Pérez-Fernández, J. Guerra, L.E. Sanchez, D.Vazquez-Garcia, M. Lopez-Torres, A. Fernández, J.J.F. Sánchez. *Dalton Trans*. **2016**, *45*, 19127.

[82] J. Silva, A.S. Rodrigues, P.A. Videira, J. Lasri, A.J. Charmier, A.J.L. Pombeiro, A.R. Fernandes. *Inorg. Chim. Acta* **2014**, *423*, 156.

[83] K.T. Mahmudov, M.F.C. Guedes da Silva, A. Mizar, M.N. Kopylovich, A.R. Fernandes, A. Silva, A.J.L. Pombeiro. *J. Organomet. Chem*. **2014**, *760*, 67.

[84] T.F.S. Silva, L.M.D.R.S. Martins, M.F.C. Guedes da Silva, M.L. Kuznetsov, A.R. Fernandes, A. Silva, C-J. Pan, J.-F. Lee, B.-J. Hwang, A.J.L. Pombeiro. *Chem.- An Asian J.* **2014**, *9*, 1132.

[85] R. Vinhas, A.R. Fernandes, P.V. Baptista. *Mol. Ther. Nucleic Acids*, **2017**, *7*, 408.

[86] J. Schindelin, I. Arganda-Carreras, E. Frise, V. Kaynig, M. Longair, T. Pietzsch, S. Preibisch, C. Rueden, S. Saalfeld, B. Schmid, J.Y. Tinevez, D.J. White, V. Hartenstein, K. Eliceiri, P. Tomancak, A. Cardona. *Nat. Methods*. **2012**, *9*, 676.

[87] A. Perelman, C. Wachtel, M. Cohen, S. Haupt, H. Shapiro, A. Tzur. *Cell Death Disease*. **2012**, *3*, e430.

Graphical Abstract

The study of the biological activity of a series of ten gold(I) complexes containing the same chromophoric unit (4-ethynylaniline) and that differ on the phosphine, located at the second coordination position, demonstrated the possibility of modulating tumour selectivity and cytotoxicity depending on factors such as: nuclearity of the resulting complex (mono- or diphosphine), flexibility, solubility in water. An important factor to highlight is the fact that higher apoptosis effects can be related to an increase of intracellular ROS.

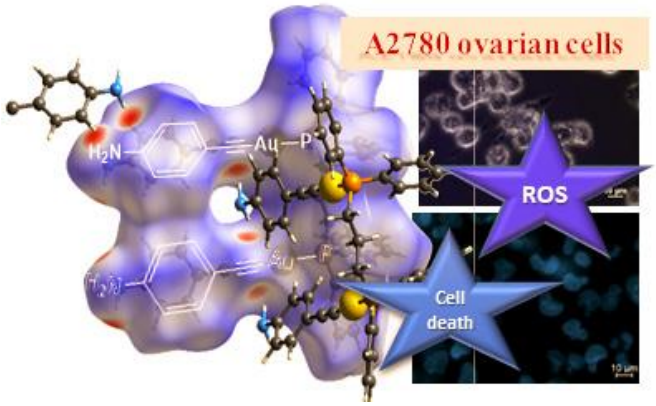

CIF

[checkCIF Results]

CIF

[checkCIF Results]

CIF

[checkCIF Results]

CIF

[checkCIF Results]

check cif

check cif

check cif

check cif

TOC